TECHNISCHE
UNIVERSITÄT
WIEN
Vienna University of Technology

MASTER THESIS

Construction and Operation of an Aerosol Test Device for Measuring the Particle Size Distribution and Collection Efficiency of Nanoparticles in Liquids

carried out for the purpose of obtaining the academic degree of a graduate engineer

submitted to the TU Wien, Faculty of Technical Chemistry

by

Andreas Strasser,
Matriculation Number: 01325112

under the Supervision of
Ass. Prof. Dipl.-Ing. Dr. techn. **Gerd Mauschitz**
Dipl.-Ing. Dr. techn. **Thomas Laminger**

Institute of Chemical, Environmental and Bioscience Engineering
Research division Mechanical Process Engineering and Clean Air Technology
TU Wien
Getreidemarkt 9, 1060 Vienna, AUSTRIA

July 30, 2020

Danksagung

Zunächst gilt mein Dank Thomas Laminger und Prof. Gerd Mauschitz die mir diese Diplomarbeit ermöglicht haben und mir über den Verlauf der Arbeit großartige Unterstützung zukommen haben lassen.

Mein großer Dank gilt meiner Mama und meinem Papa, die mir es ermöglicht haben unbeschwert, über einen relativen langen Zeitraum zu studieren. Darüber hinaus danke ich meiner ganzen Familie, die mir immer mit Rat und Tat zu Seite gestanden ist oder mir eine gewollte Ablenkung geboten hat.

Des Weiteren möchte ich allen meinen Freunden, speziell Anna, Martina, Veronika, Emil, Sascha und Timi danken, die das Studium in eine unvergessliche Zeit verwandelt haben, sowohl in heiteren als auch in ernsten Abschnitten.

Mein Dank gilt auch all jenen, die mich auf diesem Weg begleitet haben.

Abstract

This Master Thesis is part of the project *Entwicklung eines Lunge am Chip-Systems zur in- vitro Analyse der Toxizität von Nanostäuben*. The main goal is to transfer commercial available inorganic dusts, which consists of nano scale particles in an airborne state and collect these in an eligible liquid medium for further examination.

Therefore an aerosol test device was developed, constructed and made operational. The aerosol test rig was thoroughly tested before the first test was conducted. At first the ability to produce a stable aerosol flow was tested. Three selected test dusts (Titanium dioxide, Silicon dioxide and Zinc oxide) were dispersed with the aerosol test rig. The duration that the test device took to produce a stable aerosol flow was measured. The results show that each test dust needs a certain time till a stable aerosol flow is reached.

In addition the particle size distribution of each test dust was examined. For this purpose two different analysers were used. Both measured the newly generated aerosol at the same time. The results show that both analysers provide a similar particle size distribution, but the accuracy differ greatly with greater particle sizes.

The last experiment engages on the task of retrieving a collection efficiency for every test dust. A constant aerosol flow was provided and directed into the *Impinger*. The raw and crude gas concentration was measured. The received data was analysed and the collection efficiency was calculated. The results show that the collection efficiency is mostly depending on the particle size, but the type of material has some effect on the measurements.

Kurzfassung

Dieser Masterarbeit wurde im Zuge des Projektes *Entwicklung eines Lunge am Chip- Systems zur in- vitro Analyse der Toxizität von Nanostäuben* durchgeführt. Das Ziel ist kommerziell erhältliche anorganische Stäube, die aus nanoskaligen Partikeln bestehen, in den luftgetragenen Zustand zu versetzen und diese anschließend in einem geeigneten flüssigen Sammelmedium abzuscheiden, um diese weiteren Untersuchungen zu unterziehen.

Dafür wurde eine Testapparatur entwickelt, aufgebaut und in Betrieb genommen. Nach Überprüfung der Funktionsfähigkeit der Testapparatur wurde die Dauer bis zum Erhalt eines konstanten Aerosolstroms untersucht. Für die drei ausgewählten Teststäube (Titandioxid, Siliciumdioxid und Zinkoxid) wurden unterschiedlich lange Zeiten bis eine Konstanz des Aerosolstroms gegeben war, festgestellt.

Des Weiteren, wurden die Partikelgrößenverteilung der drei Stäube untersucht. Dabei kamen zwei unterschiedliche Messgeräte zum Einsatz die zeitgleich das generierte Aerosol vermessen haben. Die Untersuchungen haben gezeigt, dass die beiden Messsysteme, anhängig von der untersuchten Partikelgröße und dem untersuchten Material, übereinstimmende Ergebnisse liefern. Jedoch unterscheiden sich die Resultate stark bei Partikelgrößen von über 400 nm bei Siliciumdioxid und Zinkoxid.

Im letzten durchgeführten Experiment wurde die Sammeleffizienz eines Waschflaschen-Systems, genannt *Impinger*, untersucht. Dabei wurde ein konstanter Aerosolstrom bereitgestellt und dieser dann in einen mit Glaskörpern und destilliertem Wasser gefüllten *Impinger* eingeleitet. Die Roh- und Reingaskonzentrationen wurden bestimmt. Anschließend wurde rechnerisch ein Abscheidegrad berechnet. Die Berechnungen haben gezeigt, dass die Sammeleffizienz maßgeblich von der abgeschiedenen Partikelgröße abhängt und von der Art des Materials.

Contents

List of Figures

1 Introduction

Ultra fine dusts with particle sizes smaller than 100 nm are the main subject of numerous research projects. It is important to research the interaction of fine dusts with the human respiratory system, because there are plenty of examples, where the inhalation of fine particles can cause serious damage to the human health.

Therefore the project *Entwicklung eines Lunge am Chip-Systems zur in-vitro-Analyse der Toxizität von Nanostäuben* was launched. The overall goal of the project is to develop a tool to examine the harmful potential of nano scale dusts on human cells. Therefore it is necessary to simulate the natural conditions of airborne nano scale particles under laboratory conditions. Hence dust samples have to be finely dispersed and collected into a lung fluid substitute without altering the particle size distribution of the nano scale materials.

The project is split into five consecutive work packages. The first package consists of project management and organisational tasks. The second package is the first research related part. The main goals are, collect data and characterize industrial used particles, produce stable and applicable particle suspensions and determine the oxidative stress on acellular tests. Identification of macrophages suitable for co- cultivation for A549 cells, which is a type of cancer cell mostly used to study lung cancer and for drug development, over a period of 72 hours, is the task of the third work package. Lung on a chip development and long time testing, regarding cytotoxicity are the main goals for the fourth and fifth work packages.

1.1 Aim of the work

This master thesis engages on the task of developing an aerosol test device to examine commercial available inorganic powders (Titanium dioxide, Silicon dioxide and zinc oxide), which consists of nano scale particles. The test rig should be

able to transfer these dust samples into an airborne state and the newly generated aerosol should be dispersed into a liquid medium. The aerosol test rig should be able to provide a variety of different aerosol concentration and is able to uphold a constant aerosol flow.

Furthermore the aerosol test rig should be equipped with sufficient analysing equipment to measure and monitor concentration and particle size distribution of the aerosol before and after the deposition of particles into the dispersant.

In addition the collection efficiency of solid particles in a dispersant should me measured and discussed.

1.2 Background

Since the dawn of mankind particles of different shape and size have always surrounded us, in the air, water and soil. Till the recent centuries the origin of the these particles have been natural ones, but with the beginning of the industrial revolution mankind started to put a constant flow of man made particles into our environment. The effects on the human body, regarding fine particles can be a problematic one, if these are not well handled. Technology made great advancements in preventing fine particles to slip into the air, hence detaining them to circle around in our ecosystem. The most researched ones and publicly denounced are the residues from combustions processes. These particles caused a series of incidents, e.g. the Great Smog from 1952, these are the main reason for clean air technology advancements. During the second half of the 20th and the beginning of the 21st century strict rules for emission limits were established to ensure a safer handling. But there are far more common used fine particles, besides combustion residues. Titanium dioxide , Silicon oxide and Zinc oxide are used on an industrial scale, but there is far lesser knowledge on their interaction with the human body and our ecosystem than their combustion counterparts. Therefore it is necessary to determine the toxicological properties of these particles.

The greater goal is to eliminate any man made air pollutant emissions, therefore strict regulations were established by the Austrian government.

Immissions limits		
Pollutant	Concentration [µg/m^3]	Averaging Period
SO_2	120	daily mean value
PM_{10}	50	daily mean value
PM_{10}	40	yearly mean value
$PM_{2,5}$	25	yearly mean value
CO	10^4	moving eight- hourly average
NO_2	200	half- hourly average
Benzol	5	yearly mean value
Lead	0,5	yearly mean value

Table **??** shows some selected air pollutants and their immission limit. [34]

Furthermore studies show that some particles can cause inflammatory reactions and are cytotoxic, for example the Department of Biological Sciences of the Boise State University conducted experiments on the toxicity of zinc oxide. The paper shows that zinc oxide nanoparticles cause a cytotoxic reaction and that the toxic abilities of zinc oxide nanomaterial should not be neglected. In addition the finding of this paper must be considered for the potential incorporation of ZnO nanoparticles into novel nanotechnology-based biological applications. [15]

Regarding Titanium dioxide nanoparticles, there are a lot of papers available, that suggest the harmful effects of nanoparticle exposure to animals, such as rats [9] and rainbow trout [11], not only as airborne particles, but as suspended particles too.

1.3 On Dust and Particles

Dust consists of a number of fine solid particles. Particles have varying origins such as, natural occurrences, for example erosion, Vulcanian activity, and so on and man made, for example combustion residues and attrition. As varying as the origins of particles are, even more wide ranging are their components. The composition of ordinary house dust consists of biological matter, like pollen, hair and different fibers and of non biological origin, such as pharmaceuticals, drugs, explosives and minerals. [16]

Dust that is wind borne and that takes a long time to settle down is called

atmospheric dust. A part of these particles are from remarkable interest for mankind, in particular the particular matter 10 (PM_{10}) and 2,5 ($PM_{2,5}$), which is a subset of PM_{10}.

The U.S. EPA defines PM_{10} ($PM_{2,5}$) as particulate matter with a diameter of 10 (2.5) micrometers collected with 50% efficiency by a PM_{10} ($PM_{2,5}$) sampling collection device. [36]

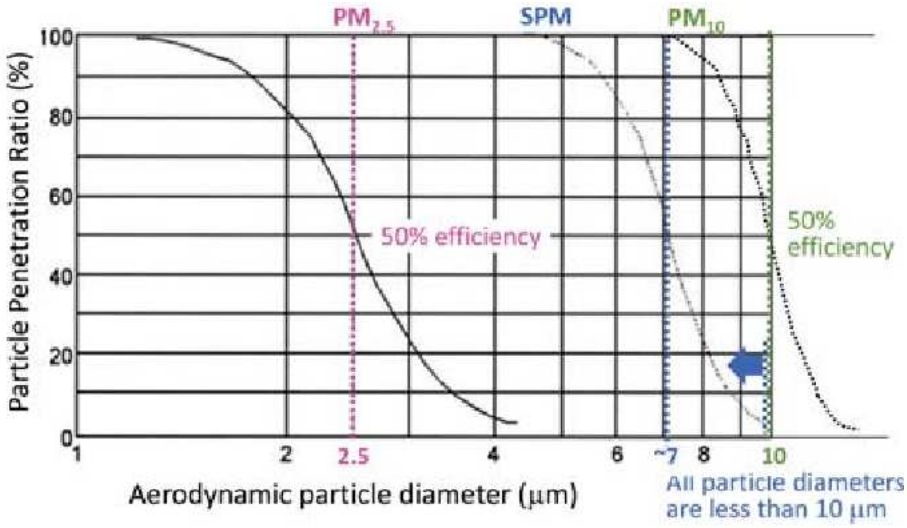

Figure 1.3.1: Illustrated Definition of $PM_{2,5}$ and PM_{10} [36]

Figure 1.3.1 shows the separation curve for selected airborne particle sizes, in regard of the their ability to penetrate the human respiratory system.

These two groups of particulates are respirable, meaning that these fine particles can follow the airflow directly into our alveoles, consequently being a health hazard. Therefore the $PM_{2,5}$ and the PM_{10} were listed as Group 1 carcinogens by the World Health Organisation. [12]

1.3.1 Definition and Origin of Nanoparticles

Nanoparticles made their way in our everyday lives in the past 30 years, as a food additive, hardener for synthetic materials or as transport vehicle for advanced pharmacological products. Their applicability and their suitability arises from their chemical and physical properties. The main attribute is the shape, including

surface area, morphological substructures. The particles can be modified to enhance their chemical properties, such as stabilisers against coagulation, or their physical properties, such as magnetic and electrical characteristics. [28]

The International Standards Organization (ISO) technical specification 80004-2 states that a nanoparticle is an object with all three external dimensions in the nanoscale, whose longest and shortest axes do not differ significantly, with a significant difference typically being a factor of at least 3. [13]

There are two fundamental different approaches to produce nanoparticles, Top-Down versus Bottom- Up. On one hand there is growth and self assembly, from the bottom up, involving single atoms and molecules. On the other hand there is the top- down approach in which the powerful techniques of lithography and etching start with large uniform pieces of material and generate the required nanostructures from them. Both methods have inherent advantages. [28]

The most produced fine particle pigment, which includes nanoparticles, is titanium dioxide, which will serve as an example of industrial scale NP- production. The processes, which lead to fine titanium dioxide dust material, are bottom- up techniques, the two are presented in the following part.

In 2017, more than 15 million tonnes of ilmenite, rutile, and titanium slag were processed worldwide. About 60% thereof were utilized for the production of pigments. For other end products, such as technically pure titanium, electrical conductors, and chemical intermediates, about 7% were utilized. The rest, about 33% were used for further refinement into synthetic rutile and titanium slag. [8]

Titanium dioxide occurs in nature as ilmenite, rutile or anatase, all three are minerals. The minerals are processed to produce pure titanium dioxide. The two major procedure are the chloride and the sulfate process. Furthermore the ilmenite is processed to rutile, which serves as a white pigment and is the biggest application of titanium dioxide. In addition the sulfate process can produce anatase, which is used in textile industry.

The chloride process consists of two steps.

$TiO_2 + 2\,C + 2\,Cl_2 \rightarrow TiCl_4 + 2\,CO$

$TiCl_4 + O_2 \rightarrow TiO_2 + 2\,Cl_2$

The first step, the chlorination is carried out at a temperature of about 1000°C in a fluidized bed reactor in the presence of coke. The resulting gas stream contains

$TiCl_4$, oxides of carbon and all the impurity metals from the feedstock in the form of metal chlorides. The gas stream is contacted with recycled liquid $TiCl_4$, which cools it to a level at which the other metal chlorides separate out as solids. The $TiCl_4$ goes forward with further cooling to be condensed as a liquid and is then fed to a high temperature oxidation reactor where it is reacted with oxygen in a plasma reactor or toluene burner to re-form TiO_2 and release the chlorine which is recycled back to the beginning of the reaction. This pure TiO_2 is subjected to a range of chemical surface treatments and milling and drying operations to give a range of products with particular properties in terms of dispersion and durability, suitable for various end use applications. [27]

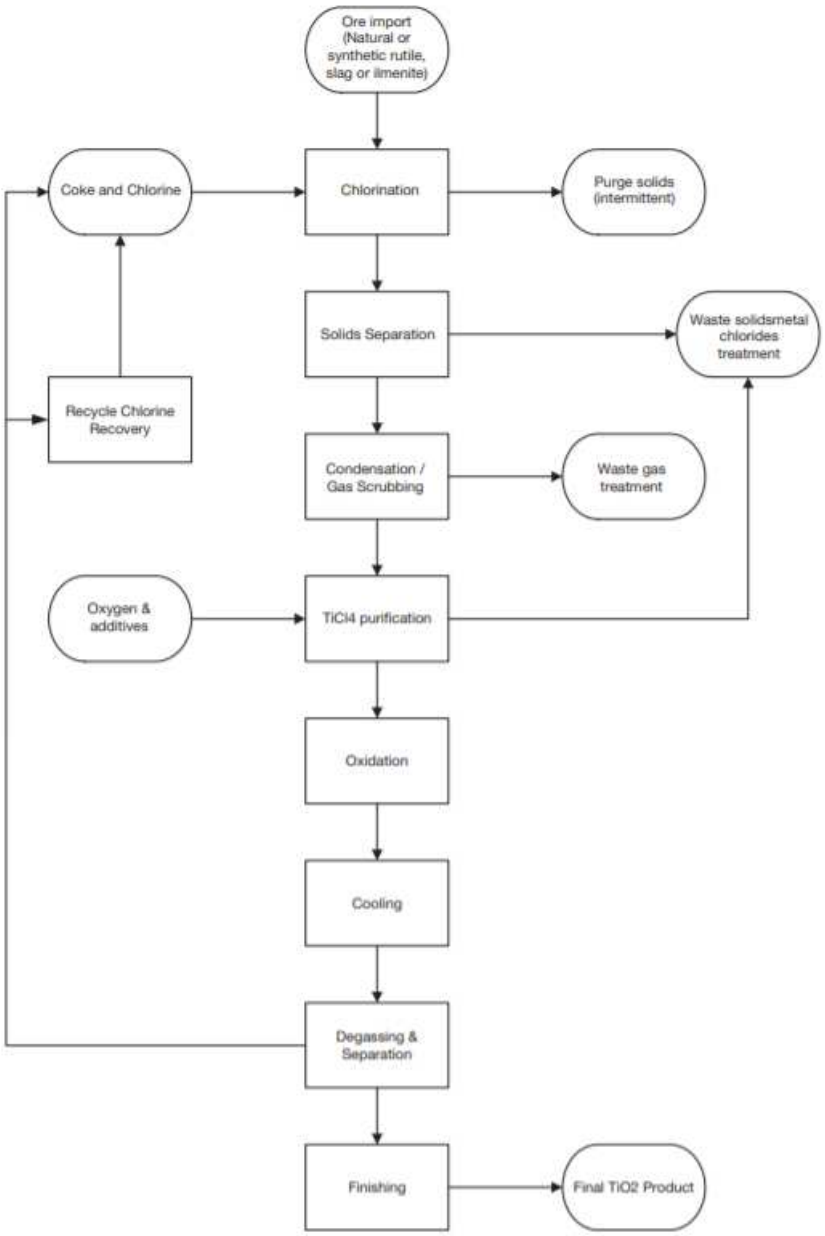

Figure 1.3.2: Flow Chart of the Chloride Process [27]

The second one is the sulphate process.

$FeTiO_3 + 2\,H_2SO_4 \rightarrow TiOSO_4 + FeSO_4\downarrow + 2\,H_2O$

$TiOSO_4 + 2\,H_{20} \rightarrow TiO(OH)_2 + H_2SO_4$

$TiO(OH)_2 \rightarrow TiO_2 + H_2O$

$Fe_2(SO_4)_2 + SO_2 + 2\,H_2O \rightarrow 2\,FeSO_4 + 2\,H_2SO_4$

$2\,FeSO_4 + SO_2 + O_2 \rightleftharpoons Fe_2(SO_4)_3$

$2\,H_2O + 2\,SO_2 + O_2 \rightleftharpoons 2\,H_2SO_4$

The feedstock is first digested in strong sulphuric acid which converts the titanium components into titanyl sulphate and the iron into sulphates. Where the feedstock used is ilmenite based, a reduction step is required in which iron is added to convert any ferric iron to the ferrous form to aid separation later in the process. This is followed by a clarification step to remove any undigested material from the liquid. For an ilmenite process, crystallization typically follows, which separates out the co-product ferrous sulphate heptahydrate (copperas), though it is also possible to extract copperas later in the process. Copperas is sold for a range of applications including water treatment, agriculture and use in cement. The liquor passes forward to a hydrolysis stage in which the oxysulphate is reacted with water to produce a hydrated titanium dioxide product and releases sulphuric acid. The hydrated TiO_2 passes forward to a rotary kiln where it is calcined to produce the anhydrous titanium dioxide product. Further processing (finishing), is then analogous to the chloride process involving chemical surface treatments (coating) and milling and drying operations. The acid that is released at hydrolysis is not strong enough to be used directly in the digestion step, so it is subject to one of two processes, either acid concentration or neutralization (to produce gypsum). In the former, the acid is typically subjected to a number of heating, concentration and filtration cycles to increase the strength of the acid to a level allowing reuse in the process or sale. The process also concentrates residual iron that is separated as a ferrous sulphate monohydrate co-product. The alternative process, involving gypsum production, treats the acid with a calcium salt to give gypsum, which is used in plasterboard manufacture, agriculture and cement. [27]

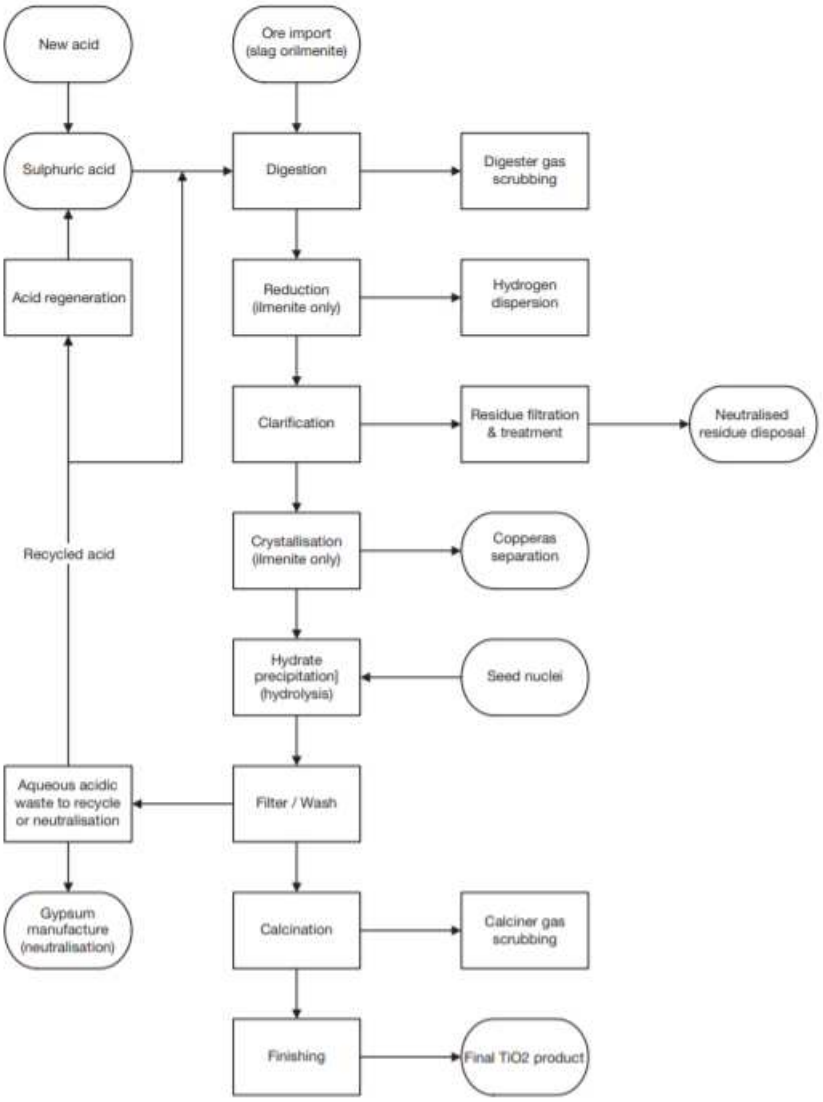

Figure 1.3.3: Flow Chart of the Sulphate Process [27]

There are other major industrial produced particles, for example silicon dioxide or aluminium dioxide. All of them can have negative effects on the environment and the ecosystem, hence are harmful towards human and animal live. Therefore a constant increase in industrial production of nanoparticles, should always be accompanied by an increase in safety standards and awareness of the risk we, as humanity are exposed to.

1.4 Basic principles

1.4.1 Particle characteristics

Particles come in all form and shapes, therefore it is necessary to describe properties and features of a certain particle collective with measurable parameters, with the least amount of parameters necessary. Particles that can be described completely with one parameter, such as cubes, tetrahedrons, octahedrons and so one, are not common in the field of particle analytics. Sometimes particles can be described with two geometrical parameters. Most of the time particles are irregularly shaped. There are two approaches to determine the preferable parameter to describe the particle collective, at first it is possible to use a fitting shape to describe the collective as a whole. For example the particles are described as a sphere or an ellipsoid. The second approaches is to use the parameter that is provided by a certain measurement technique. For example the hydrodynamic diameter, when using dynamic light scattering, to determine the mean particle size in suspension.

In the following part, different parameters to describe the properties and/or features of a particle collective are shortly described.

Length

The most common used therm to describe particles is the length, but it is referred to as particle diameter or particle size. Most of the time. particle analysers use statistical diameters, which are related to the measuring direction, these have different definitions.

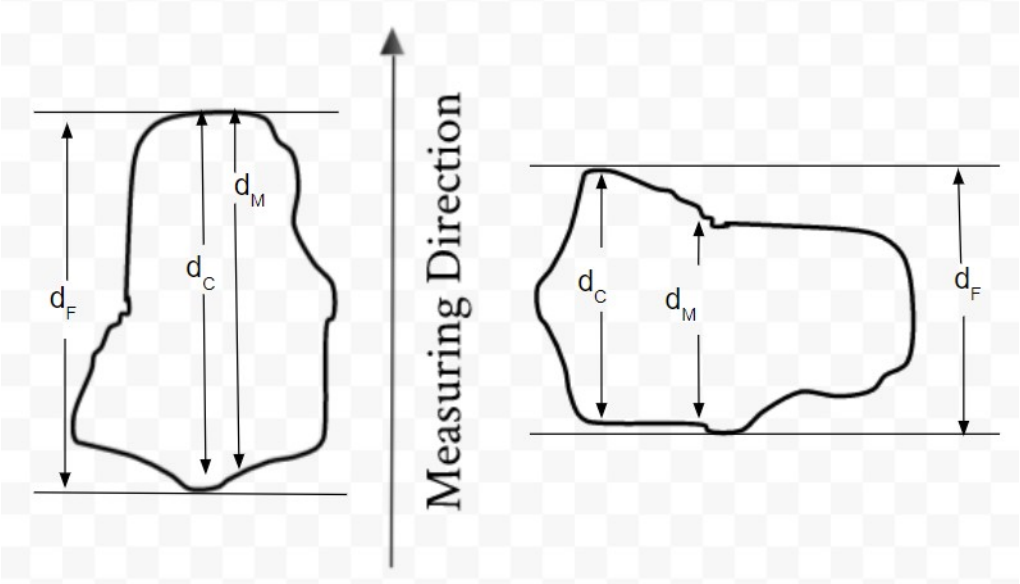

Figure 1.4.1: Different Statistical Diameters exhibited on a Particle

Figure 1.4.1 shows different statistical diameters. d_F is the Feret- diameter, which is defined as the distance between two parallel tangents, that restrict the outlines of the particle. d_M is the Martin- diameter, which cuts the projection area of the particle in two equal sized areas. d_C is the longest chord in measuring direction. [17]

Surface

Another common parameter to characterise a particle is the surface. In general it is not possible to measure the surface area of every particle, but the Cauchy theorem established a link between the mean projection area A_m and the surface area S, the result is shown in formula 1.1. [17]

$$S = 4A_m \tag{1.1}$$

Volume

A well known measuring technique, the Coulter- Counter, retrieves a signal proportional to the particle volume. The main advantages is that the particle characteristic volume is not dependant on the measuring direction.

Other particle characteristics are the mass, equivalent diameter and the rate of descent.

1.5 Scanning mobility particle sizer

The Scanning Mobility Particle Sizer, short SMPS, is an analyser for aerosols, regarding their particle size, surface, mass and number. Furthermore the particle feature, which is measured is the electrical mobility. The electrical mobility is the ability of a charged particle to move through a medium with an electrical field, which applies a force onto the particles. The SMPS consists of two major system, first to determine the particle size, the Differential Mobility Analyser (DMA) and second to determine the particle concentration, the Condensation Particel Counter (CPC). This system was extensively used for this Master thesis, therefore it is important to understand how the SMPS works and which parameters effect an aerosol measurement.

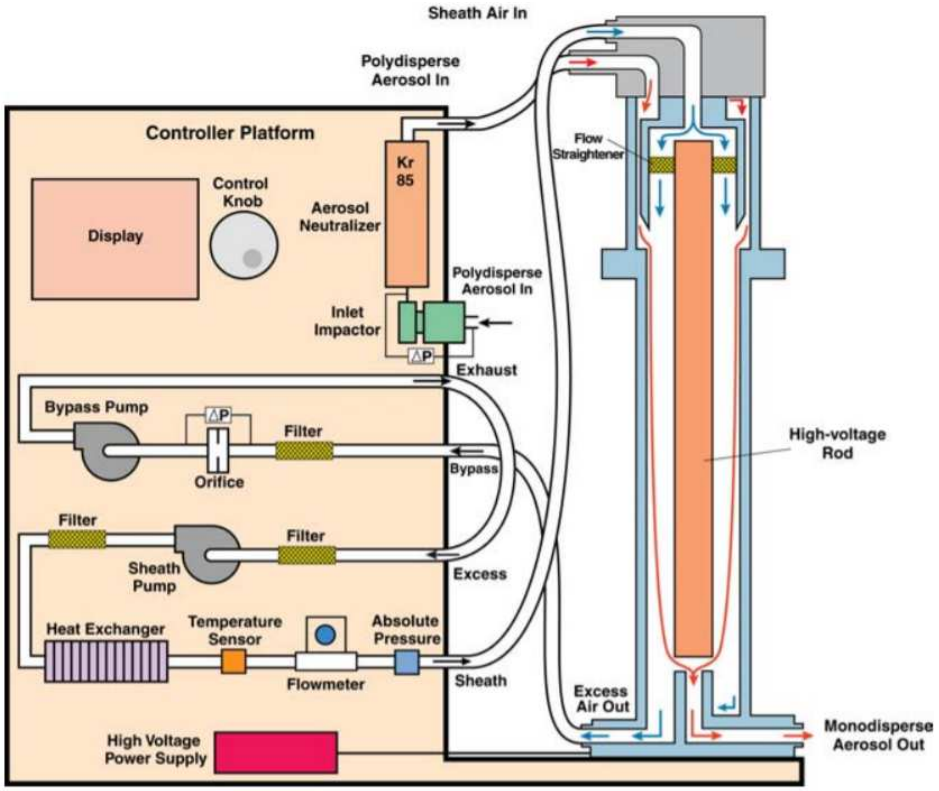

Figure 1.5.1: Scheme of the TSI 3080 SMPS without the CPC [33]

Figure 1.5.1 shows a scheme of the SMPS without a particle counter unit, that was used throughout this thesis. Furthermore the picture shows the stages that a poly disperse aerosol traverses, when flowing through a SMPS. At first the poly disperse aerosol passes by a single- level impactor to get rid of particles bigger, than 1 µm. Then the aerosol enters the neutralizer. Afterwards the aerosol is classified in the electrostatic classifier of the DMA. A mono disperse aerosol exits the DMA and is directed into a particle counter unit to determine concentration and number of a given aerosol sample.

In the following passage, every step that the aerosol passes through is further explained.

1.5.1 Neutralizer

All natural and man made particles carry charges. The forces between two charged particles are far greater than any other force. Therefore it is important to understand what effects causes particles to obtain charges and how to affect these charges. There are some major effects that cause particle charges, some of them are shortly presented, the tribolectrical effect, the bipolar diffusion charging, the unipolar diffusion charging, field charging, Thermal, Chemical and Photoionization.

The kinetic theory of gases provides the answer to the number of charges n_D that changes over time on a given particle, due to diffusion.

$$\frac{dn_D}{dt} = \frac{\pi \bar{c}}{4} N_I d_p^2 exp(\frac{n_D e^2}{2\pi\epsilon_0 d_p kT}) \tag{1.2}$$

In formula 1.2 n_D is the number of charges, t is the time, $\bar{c}$ is the mean thermal velocity of ions, k is the Bolzmann constant, T is the absolute temperature, d_p is the particle diameter, N_I is the concentration of ions in the charging area, e is elementary charge and ϵ_0 is the vacuum permittivity.

After the charging time t_c an uncharged particle receives, according to formula 1.2, the mean number of elementary charges n_D. [32]

$$n_D = \frac{2\pi\epsilon_0 kT}{e^2} d_p ln(1 + \frac{\bar{c}e^2}{8\epsilon_0 kT} d_p N_I t_c) \tag{1.3}$$

Triboelectrical Effect

The triboelectrical effect is a mechanism, where certain materials get electrically charged after contact and separation, due to the difference in work function of both materials. The magnitude of the effect is affected by contact area, existing charges and material properties.

A well known example for the triboelectrical effect is charging a balloon by rubbing it on synthetic textiles.

Bipolar Diffusion Charging

The common used method to charge particles with this effect, is to use a radioactive isotope, for example Krypton- 85. ($^{85}_{36}\mathrm{Kr} \xrightarrow{\beta-} {}^{85}_{37}\mathrm{Rb} + {}^{0}_{-1}\mathrm{e}$)

The aerosol flows past a radiation source. The radioactive element ionizes the carrier gas molecules and the available water molecules. Positive and negative charged molecules are produced, both negative and positive charged ions attach themself to aerosol particles. The number of bipolar charged particles attached to the aerosol increase over time and outnumbering the charges that were already attached to the aerosol prior to the radiation source. [32]

After sufficient long dwell time a stationary condition is reached, the Fuchs state of charge. N. A. Fuchs developed a model for the state of charge of aerosol particles in a bipolar ionic atmosphere. The main idea is, that after a certain time a stationary state must be established in which the number of particles with i elementary charges (i is a whole positive or negative number) capturing in a unit of time an ion of the same sign is equal to the number particles $i + 1$ charges capturing an ion of the opposite sign. In addition, he showed, that depending on the particle size the model to describe the state of charge of an aerosol particle has to be adjusted, resulting in the inclusion of the differential equation for the diffusion of gaseous ion of a certain sign towards a spherical particle in the absence of an external field. [14]

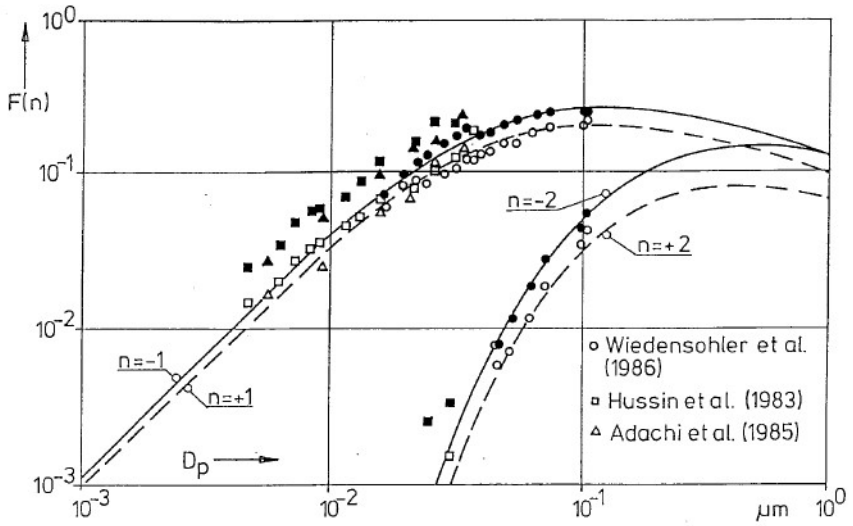

Figure 1.5.2: Bipolar State of Charge in Air [26]

Figure 1.5.2 shows the charge distribution of an aerosol in dependency of the particle diameter at the exit of the neutralizer. The drawn through lines depicted

the theoretical calculations of Fuchs. The squares, triangles and circles are the experimental results of the stated authors. The white filled symbols are positively charged and the black filled symbols the negatively charged particles. The upper curves show the single charged particles and the lower curves show the double charged particles. The picture clearly shows that the model calculations match with the experimental findings.

Diameter [nm]	Fraction of Particles with n Elementary Charges										
	-5	-4	-3	-2	-1	0	+1	+2	+3	+4	+5
1,0	0,00	0,00	0,00	0,00	0,11	99,79	0,10	0,00	0,00	0,00	0,00
2,0	0,00	0,00	0,00	0,00	0,34	99,73	0,29	0,00	0,00	0,00	0,00
5,0	0,00	0,00	0,00	0,00	1,40	97,42	1,18	0,00	0,00	0,00	0,00
10,0	0,00	0,00	0,00	0,00	3,98	92,71	3,31	0,00	0,00	0,00	0,00
20.0	0,00	0,00	0,00	0,02	10,03	81,80	8,14	0,01	0,00	0,00	0,00
50,0	0,00	0,00	0,01	1,02	22,09	58,69	17,56	0,63	0,00	0,00	0,00
100,0	0,00	0,01	0,35	5,39	27,00	42,70	21,12	3,28	0,16	0,00	0,00
200,0	0,04	0,47	3,18	12,08	25,58	30,13	19,72	7,17	1,45	0,16	0,01
500,0	2,22	5,33	10,19	15,51	18,79	18,13	13,93	8,52	4,15	1,61	0,50
1000,0	6,53	9,23	11,64	13,14	13,24	11,94	9,62	6,92	4,46	2,56	1,32

Tabular 1.5.1 [26] shows the results of charged particles in dependency of the particle diameter according to the findings of Fuchs. For small particles up to 50 nm, most particles out of an aerosol sample carry zero positively or negatively charged elementary charges.

Unipolar Diffusion Charging

The unipolar diffusion charging is similar to the bipolar diffusion charging, but the positive and negative charged ions get separated. An electric field separates the charged ions, hence only one species of ions remains to get attached to aerosol particles.

Due to the electric field, charged aerosol particles, especially small particles, are drawn away from the main aerosol flow, therefore countermeasures were developed.

Corona Discharge Charger

One type of unipolar diffusion charger is the corona discharge charger. Corona discharge is produced by a non-uniform electrostatic field such as that between a needle and plate or a concentric wire and a tube. Air and other gases can undergo electrical breakdown when the electric field strength is high. For the case of the wire and the tube, the only place this breakdown can occur is in a very thin layer at the wire surface. In this corona region, electrons have sufficient energy to knock an electron from gas molecules creating positive ions and free electrons. During this process, aerosol flow is directed across the corona discharge field and is charged by random collisions between the ions and particles due to Brownian motion of ions in space. [20]

In the corona-needle chargers, Whitby (1961) developed the first needle-type corona charger as shown in figure 1.5.3, which was capable of converting the corona current into free small ions with 100% efficiency. It consisted of an arrangement of a sharp needle held at high potential upstream of a small sonic orifice to generate the ions within a non-conductive housing. Clean air entered at the inlet and then passed through the orifice plate. Positive, negative, or alternating current voltages on the needle electrode with respect to the orifice plate were used to produce positive, negative, or a mixture of positive and negative ions. It was reported that the ion generator produced unipolar or a mixed positive and negative ion concentration of up to 10^{11} ions/cm^3 in the charging zone, and total ion outputs of 10^{14}/s. [20]

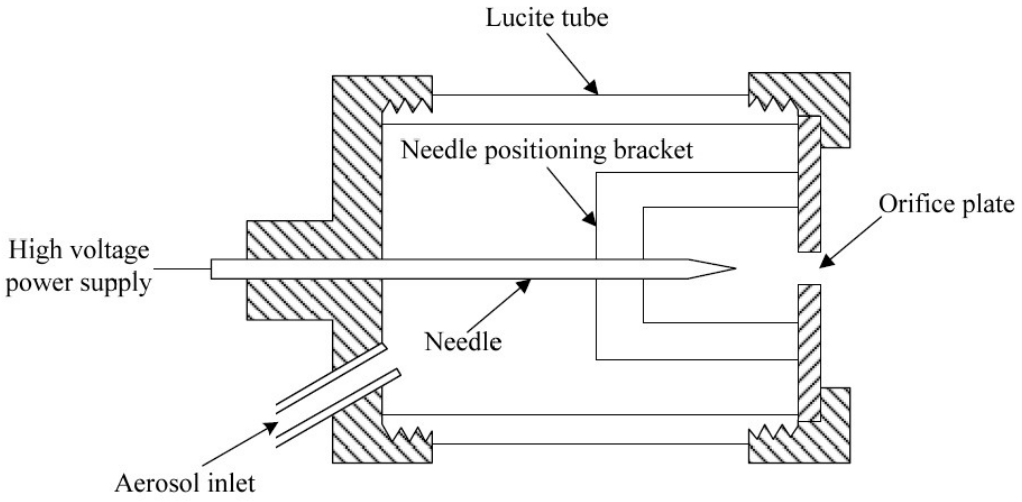

Figure 1.5.3: Schematic diagram of the sonic jet ion generator developed by Whitby (1961) [20]

Field Charging

Field charging is a from of charging an aerosol, that occurs when traversing through an unipolar diffusion charger. Charging of particles in unipolar gaseous ion density is usually described in terms of diffusion charging (effect of thermal agitation of ions, preponderant for small particles and/or low applied electric fields and field charging preponderant for larger particles and higher electric fields (effect of ion flux due to an applied electric field). [35]

On the one hand unipolar diffusion charging has advantages over bipolar diffusion charging, it does not reach an equilibrium charge distribution, thereby enabling the attainment of a higher charging efficiency. Additionally, it can grow by Brownian coagulation in the bipolar diffusion charging if the aerosol particle number concentration is above about $10^7/\mathrm{cm}^3$. [20] In addition the import of radioactive materials is often a problem, resulting in long and wasting processes to gain a permission from the particular government.

On the other hand bipolar charging is a cheap and reliable source of charging, only limited by the half life of the radioactive isotope, that is used.

Thermal Ionization

Thermal Ionization is a form of surface ionization. A particle of low ionization potential I_i can be ionized by contact with a surface of high work function ϕ that is hot enough to thermally evaporate the particle in ionic form. In this process, a valence electron of the adsorbed atom or molecule is lost to the surface upon evaporation or desorption of the positive ion. [6]

Chemical Ionization

A chemical ionization (CI) source is described in which the reagent gas is ionized by a Townsend discharge, which is a gas ionization process, rather than by high energy electrons emitted from a hot metal filament. This new source can be employed to generate both positive and negative CI spectra with comparable sensitivity using a wide variety of both oxidizing and reducing reagent gases. [18]

Photoionization

Photoionization is a process. where a photon interacts with an atom or a molecule and creates an ion.

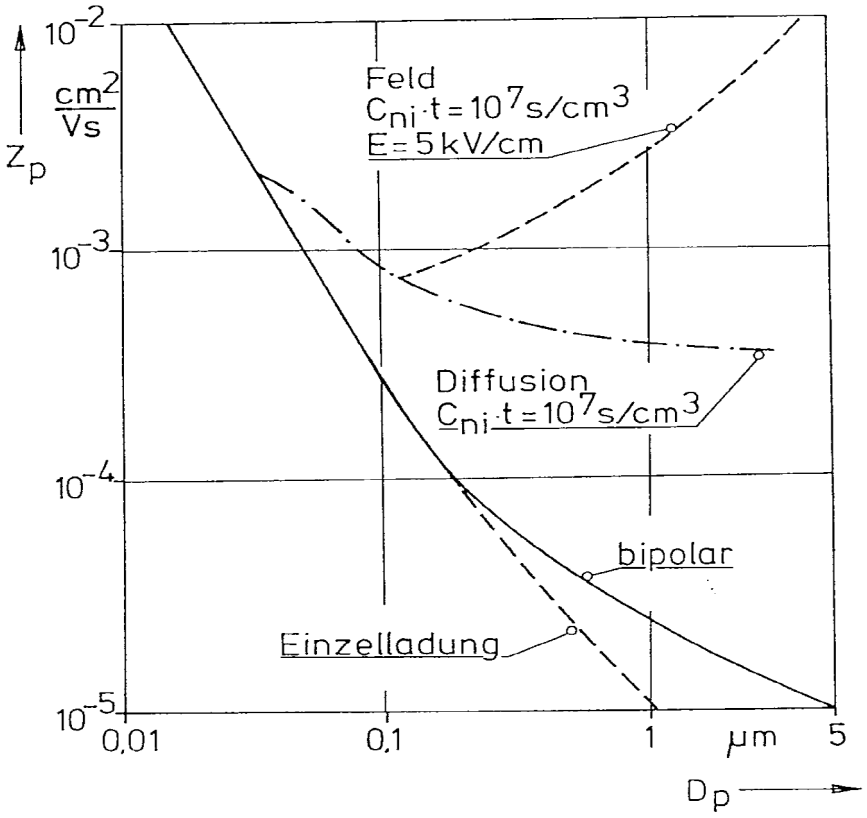

Figure 1.5.4: Electric mobility as function of the Particle Diameter D_p [26]

Figure 1.5.4 shows that different kind of charging processes have an impact on the ability of charged particles to travel through an electric field. Furthermore the charging processes are not equally effective in regard of the particle size. As an example bipolar diffusion charging has a better ability to charge smaller particles, but the efficiency decreases rapidly compared to to unipolar diffusion charging in dependency of the particle size.

1.5.2 Electrostatic Classifier of the Differential Mobility Analyser

The DMA is part of the SMPS and is a particle classifier, which lets particles move according to their electrical mobility, which is the ratio of the particle velocity and the causative electric field. The DMA is a cylindrical capacitor with an inner and an

outer electrode. [4] The incoming aerosol flow is injected into a stream of laminar particle free air, called sheath air. The sheath air accomplishes two important tasks, at first it enables charged particles to traverse the electrostatic classifier, because in the absence of any air flow all charged particles would inevitable travel to one of the electrodes. Secondly, the particle free air flow can be adjusted to enhance the effectiveness of the classifier, resulting in slower or higher flow rates, depending on the particle size. The sheath air passes through a high-efficiency particulate air (HEPA) filter and is then introduced to the aerosol.

Then the polydisperse aerosol travels through a slotted nozzle. Right after the entry into the capacitor chamber the charged particles are effected by the electrical field. The electrical field can be changed to classifier different particle sizes. Normally the SMPS measures through all size class, one after another the DMA changes the electrical field accordingly. The rod voltage and the sheath air flow rate are the primary settings that controls the particle size exiting the DMA. [33]

The aerosol surrounds the inner core of sheath air, and both flows pass down the annulus with no mixing of the two laminar streams. The inner cylinder, the collector rod, is maintained at a controlled negative voltage, while the outer cylinder is electrically grounded. This creates an electric field between the two cylinders.

The electric field causes positively charged particles to be attracted through the sheath air to the negatively charged collector rod. Particles are precipitated along the length of the collector rod. The location of the precipitating particles depends on the particle electrical mobility, the Classifier flow rates, voltage and the geometry. Particles with a high electrical mobility are precipitated along the upper portion of the rod; particles with a low electrical mobility are collected on the lower portion of the rod.

Particles within a narrow range of electrical mobility exit as a monodisperse aerosol through a small slit located at the bottom of the collector rod. The concentration of these particles can now be determined by an optical analysers or a Faraday cup. The remaining particles are removed from the classifier via the excess air flow. [33]

A scheme of the DMA is depicted in figure 1.5.5.

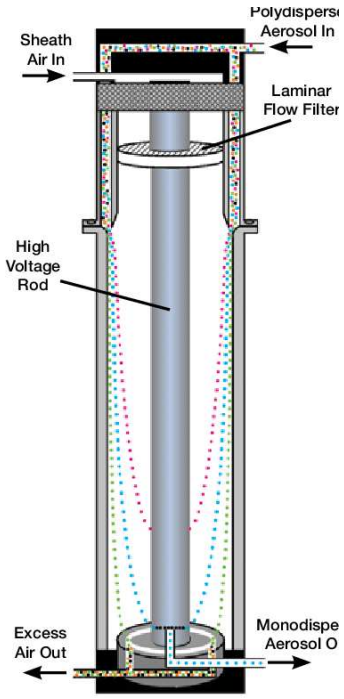

Figure 1.5.5: Schematic of the DMA[30]

The interaction between a charged particle and a electrical field, is described by following formulas.

$$F_E = Eq = Ene \tag{1.4}$$

In formula 1.4 F_E is the resulting electrostatic force of electrical field E and particle charges q, which is further distinguished with n the integer factor and e the elementary charge.

Due to the low diameter of the particles and the resulting low mass, the time that the particle need to accelerate to velocity can be neglected. The assumption is made that, as soon as the particle interacts with the electrical field, the force coming from the electrical field equals the drag force of the medium. [26]

These two opposing forces are put into context by formula 1.5.

$$F_E = Ene = \frac{3\pi\mu D_p v_E}{C} = F_W \tag{1.5}$$

In Formula 1.5 F_E is the electrostatic force, D_p is the particle diameter, μ is

dynamic viscosity of the carrier gas, v_E is the velocity of the particle caused by the electrostatic force, C is the Cunnigham slip correction and F_W is the drag force of the medium.

A slip correction factor is used to correct Stokes' law for the fact that the no-slip boundary condition is violated for small aerosol particles moving with respect to the gaseous medium. The Knudsen-Weber form of the slip correction is given by

$$C(Kn) = 1 + Kn[\alpha + \beta exp(\frac{-\gamma}{Kn})] \tag{1.6}$$

.

The parameters α, β, and γ are customarily those based upon the experiments reported in 1917 and 1923 by R. A. Millikan for aerosol droplets of oil. Because of differences in molecular interactions with the surfaces of solid particles and oil drops, different parameters should be appropriate for solid particles. [5]

The resulting velocity of charged particles is

$$v_E = \frac{EneC}{3\pi\mu D_p} \tag{1.7}$$

The electrical mobility of the particles is described in formula 1.8.

$$Z_p = \frac{v_E}{E} = \frac{neC}{3\pi\mu D_p} \tag{1.8}$$

The electrical mobility is described as the relation between the particle velocity and the electrical field. [26]

For a cylindrical mobility analyser the coordinate I of the place of precipitation of the particle with a given electric mobility Z_p is as following.

$$I = \frac{(\dot{V}_A + \dot{V}_R)ln(r_2/r_1)}{2\pi U Z_p} \tag{1.9}$$

In equation 1.9 $\dot{V}_A$ is the velocity of aerosol, $\dot{V}_R$ is the velocity of the sheath air, r_1 is the radius of the inner cylindrical electrodes, r_2 is the radius of the inner wall of the outer electrode and U is the voltage difference of the two electrodes. [26]

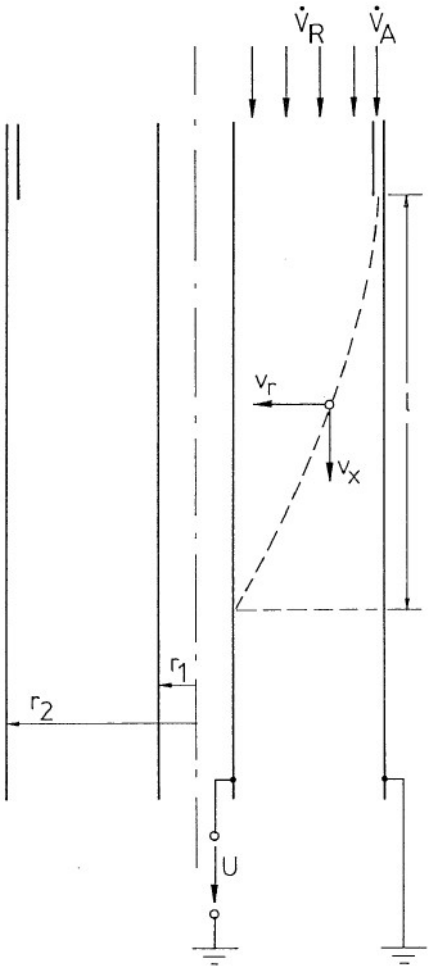

Figure 1.5.6: Scheme of a cylindrical mobility analysers [26]

Figure 1.5.6 shows the trajectory of a particle inside a cylindrical mobility analysers. Both aerosol and sheath air flow enter the analyser on top, but the aerosol enters on the outer side of the outer electrode. The particle depicted is affected by a force caused by the electric field and moves towards the inner electrode.

1.5.3 Particle Counters

The mono disperse aerosol leaves the DMA and enters a particle counter unit to determine the concentration and to receive a size distribution. Two approaches

to obtain the particle count and concentration are the Faraday cup and the condensation particle counter (CPC).

Faraday Cup

The Faraday cup is a charged particle detector. The cup consists of a field free metallic hollow body and is connected to an electrometer. The charged aerosol is directed into the cup and a charge transfer from particles to the surface of the cup takes place. The electrometer registers the change in current, when charged particles impact onto the conducting surface of the Faraday cup. The change of current is proportional to the number of particles.

Condensation Particle Counter

The condensation particle counter is an optical analyser to measure particle number and concentration. The aerosol enters the CPC and passes through a heated pipe, which is saturated with an eligible solvent, mostly alcohols. Afterwards the aerosol and the saturated air moving through a condenser. Due to the decrease in temperature, the solvent molecules start to condensate onto the aerosol particles. As a consequence the particles increase in size to around 10 µm.

The enlarged particles are directed in the measuring unit. This unit is a scattered light detector, which consists out of a light source, a measuring cell and a detector. A particle enters the measuring volume and the incoming light will be scattered in all directions and if the intensity is high enough detected. Depending on the particle size more or less light is scattered. In general small particle cause lower intensities and bigger particles cause higher intensities. To keep the CPC cost efficient, a less sensitive or cheap detector is used, hence the particle that move through the measuring volume should be big enough that the intensity of their scattered light is detected. Therefore the saturation unit after the entrance of the CPC is necessary to ensure, that even the smallest incoming particles are enlarged, thus detectable even by a low sensitivity detector.

The path of the aerosol through the CPC is depicted in figure 1.5.7.

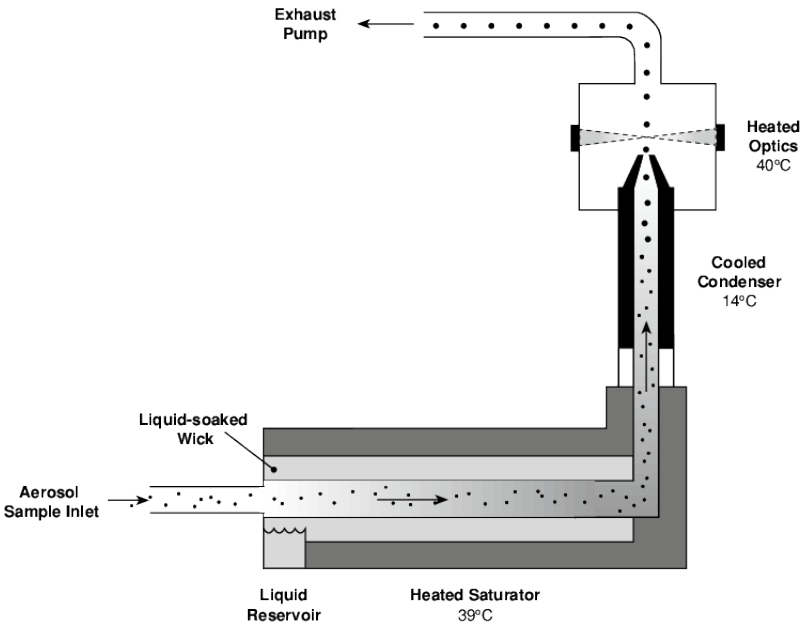

Figure 1.5.7: Scheme of the CPC [10]

1.6 Electrical Low Pressure Impactor

The ELPI+™ (Electrical Low Pressure Impactor) is a particle spectrometer for measuring airborne particle size distribution in real-time. The aerodynamic diameter is the used particle characteristic. It is defined as settling velocity of an irregular shaped particle, the test particle, which has the same settling velocity of an sperical particle with the density of 1g / cm ^{3}.

Figure 1.6.1 shows the schematic of the ELPI+, which shows the main components. The entering aerosol sample is charged via a corona discharge charger (for further explanation see section 1.5.1. The aerosol traverses after the charger through 15 impactor stages and is sized due the inertial forces of the particles.

The impactor stages are electrically insulated and sensitive electrometers are connected to each impactor stage. The charged particles collected in a specific impactor stage produce an electrical current, which is recorded by the respective electrometer channel. This current is proportional to the number concentration of particles on each impactor stage. [22]

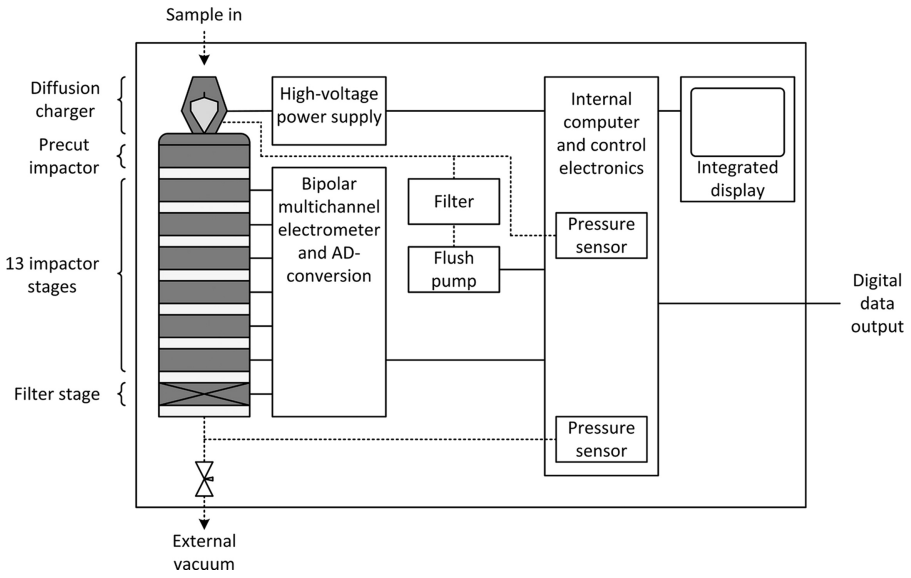

Figure 1.6.1: the schematics of the ELPI+[21]

1.6.1 Impactor

The impactor is a inertial separation device for collecting aerosol particles and to determine mass, size distribution and chemical composition of airborne particles. [24]

The ELPI+ uses an advanced version of the Berner low pressure impactor (BLPI). The Berner impactor is a modified cascade impactor.

The main principle for an impactor is: An aerosol flow is directed through a nozzle and after the distance S, the aerosol vertically hits onto a plate. As a consequence the stream is forced into a 90° turn. The inertial force drags some particles out the aerosol flow, hence an impaction onto the plate is happening. The particles that can not follow the aerosol flow are partially deposited onto the plate, this mechanism is depicted in figure 1.6.2. After a certain time the aerosol flow is turned off and the baffle plate with the impacted aerosol particle can be weighted and used for further examination.

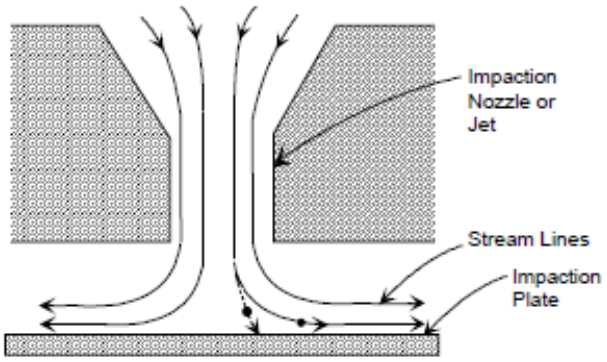

Figure 1.6.2: Scheme of aerosol impaction onto a baffle [33]

The ability of an impactor to deposit particles is described by the separation curve. The separation curve characterizes the effectiveness of a separation process of solid particles. Figure 1.6.3 shows an example of a separation curve. The ordinate is the separation function $T(d)$, a probability and the abscissa is the separation feature, in this particular depiction the particle diameter. Furthermore the diameter d_T is the particle diameter, which has a probability of 50% to be separated in this particular process.

The ideal separation curve would be a step function, hence a line parallel to the ordinate, but that is not realisable under real conditions.

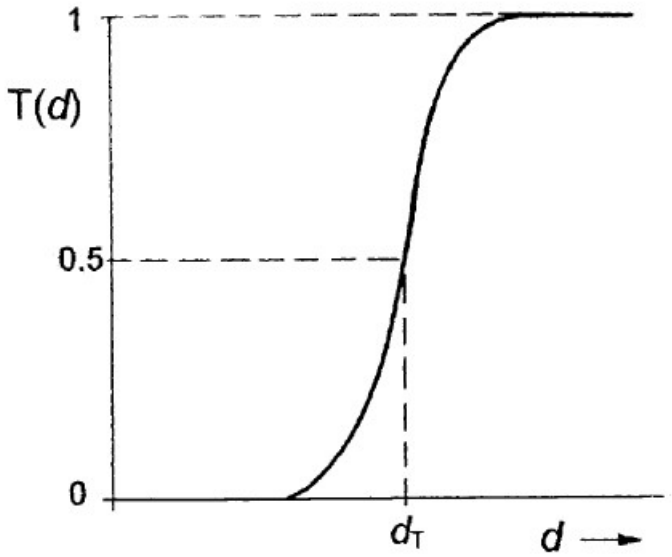

Figure 1.6.3: Example of a Separation Curve [31]

The separation curve is depending on the impactor geometry, the method of operation and particle parameters.

A successful deposition demands a contact and adhesion from particle to the plate. Thereupon a degree of separation T is received as formula 1.10.

$$T = \eta h \tag{1.10}$$

The η is the impaction ratio and h is the adhesion fraction. η can be derived from model calculations, where the particle paths are calculated with the equation of motion. Furthermore the adhesion fraction h is mainly dependent on material parameters and can not be calculated, but is derived via empirical measurements. [26]

After further examination, Virgil A. Marple found out that, the degree of separation is depending on following parameters.

$$T = T(\Psi, Re, \frac{S}{W}) \tag{1.11}$$

$$\Psi = \frac{\rho_s x^2 v}{18 \mu W} \tag{1.12}$$

$$Re = \frac{vW}{\nu} \tag{1.13}$$

Ψ is the inertia parameter in combination with the nozzle diameter W, ρ_s is the density of the solid particles, x is the particle diameter, v is the mean velocity in the throat, μ is the dynamic viscosity of the fluid and ν is the kinematic viscosity of the fluid. [25] [26]

The findings of Marple establish the dependency of impactors on the Reynolds number and the ratio between the distance of the nozzle to the baffle plate and nozzle diameter (S/W). Furthermore with a rising Reynolds number, the efficiency of an impactor increases, resulting in a sharper separation curve and the curves moves to finer particles. This phenomena is depicted in 1.6.4. The picture shows the adhesion factor on the ordinate over the inertia parameter. The nozzle form has great impact on the efficiency of the impactor, filled lines show a round nozzle impactor and the dotted curves show slot nozzle impactors.

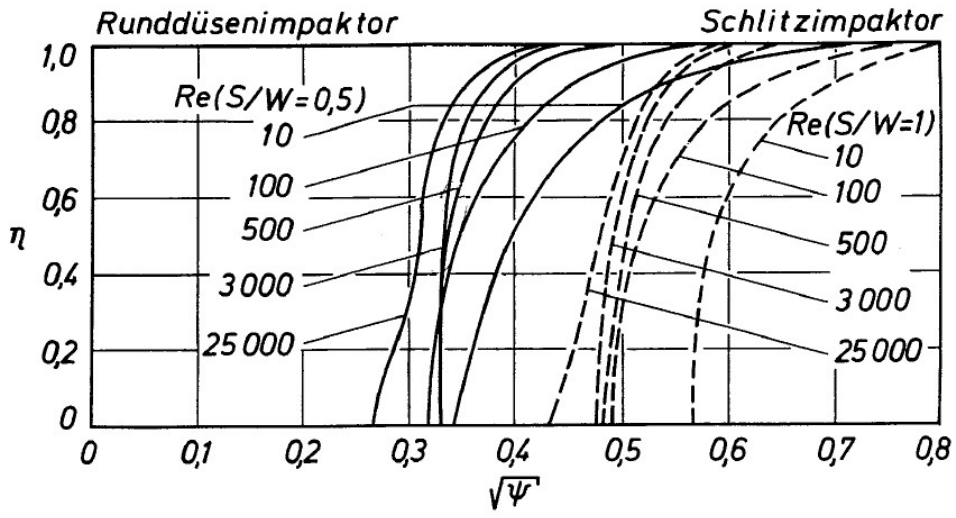

Figure 1.6.4: Dependency of the Adhesion Factor for different Reynolds Numbers [26]

To classify more than one particle size group at a time, the cascade impactor is put into use. The cascade impactor can be described as consecutive chain of separators, each impactor stage has a unique separation curve. The main idea is that the nozzle of every separator stage are getting thinner and smaller, further down the cascade impactor. Resulting in higher aerosol velocities, hence higher Reynolds numbers, which enables finer particle deposition. Modern impactor system use more than one nozzle per impactor stage to increase the precipitation quantity of aerosol particles.

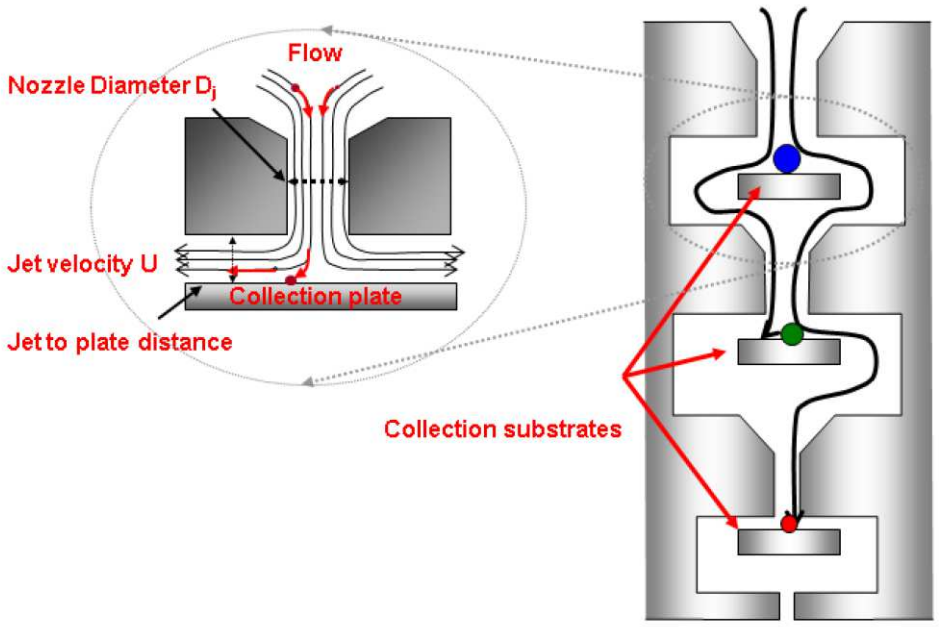

Figure 1.6.5: Scheme of a cascade impactor [22]

Figure 1.6.5 shows a scheme of a cascade impactor with three stages. Each coloured circle represents a different particle size class. The first stage separates the largest particles, presented as a blue circle. The next stages starts with a slightly smaller nozzle, deposition of the next particle size class is achieved and depicted with a green circle. This process repeats once again, the finest particles are depositioned onto the final stage, shown as a red circle.

To obtain information regarding the size distribution, mass and chemical components, each impactor stages has to be weighted and/or samples are taken. The process of cleaning and rearranging an cascade impactor is time consuming. Often quantitative measurements are not realisable due to the small particle masses that depositioned on the baffle plates during a test. Furthermore it is necessary to calibrate the cascade impactor, because the separation curves of each impactor stages have to be known to classify any given aerosol sample. The calibration is experimentally done by feeding different particle sizes to a cascade impactor, which ideally are mono disperse aerosols. The cascade impactor has fixed geometries, which are not altered during a calibration and a constant volume flow rate. For

every particle size fed to the cascade impactor a point of the separation curve is obtained.

The calibration is a time consuming process and often unwanted effects take place, that can interfere and falsify a test. For example, if the adhesion fraction is not 100%, particles that impact on a certain stage do not stick to plate, but are spread on later stages. Another common issue is that most cascade impactor tend to overload at some point into the measurement, meaning that the surface of one or more stages is completely packed with particles, preventing newly incoming aerosol particles impacting on the baffle plate and are not able to deposit on the right impactor stage. Therefore it is important to keep the particle concentration low enough, that not a single stages gets overloaded.

In addition, cascade impactors have flaws, regarding the necessity to accurately measure volume flow rates, weigh dust masses and the constant recalibrating for every new dust sample. Caused by these flaws the ELPI+ was constructed to get rid of some the major issues.

2 Experimental Set- Up

2.1 General

To simulate airborne particles an aerosol test device was built. The aerosol test device was constructed in regard of the VDI 3926 guideline.

The aerosol test device was built to assure a constant aerosol flow throughout the whole rig, therfore enabling reproducibility and repeatability for the conducted tests and experiments. Furthermore this setup was chosen because the expected particle concentrations and volume flow rates were well suited for this thesis. Two aerosol generator provide an aerosol flow for two different concentration levels, one for solid particle dispersions and the other for particles suspended in liquid. The volume flow rates are for the main pump 30 liters per minute and for the secondary pump 7 liters per minute. In addition a isokinetic sample drawing is enabled, due the positions of the probing points, around one meter after the aerosol enters the crude gas chamber.

An aerosol generator blows the particles in on the top of a approximately two meters long vertical tube. Two aerosol generators were used, the Palas RBG 2000 for high particle concentrations and for dispersing solid particle with air as a carrier gas and the Palas AGF 2.0 for low particle concentrations and for dispersing particles suspended in a liquid medium, only one generator at time was connected to the aerosol channel. The aerosol is sucked through the channel and after one meter the first probe detours some of the flow into the analysing equipment and into the *Impinger* flasks. The rest of the main aerosol is pumped into a cylindrical cartridge to prevent the solid particles from entering the ambient air and clogging the pumps. Two pumps are put into use, the first one working on higher power to maintain the main airflow through the whole device. The second pump draws air from the main air flow to feed the *Impinger* sufficient aerosol. The rest of the

secondary aerosol is pumped into a cylindrical cartridge, afterwards the cleaned air is put back into the ambient air. The two pumps are located at the bottom of the device.

The aerosol test device build for this master thesis is shown in figure 2.1.2.

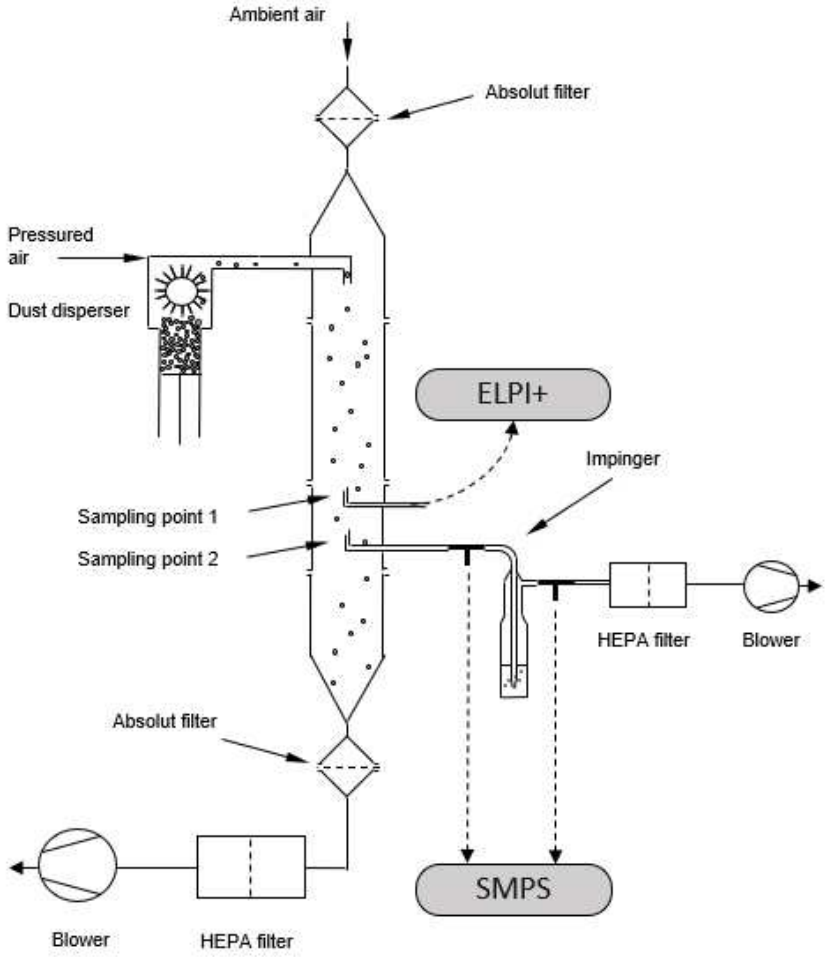

Figure 2.1.1: Scheme of the aerosol test device

Figure 2.1.1 shows a flow chart of the constructed aerosol test device. The air entrance is on top of the rig and the ambient air is cleaned by an absolute filter to prevent any ambient air particles to falsify measurements. Right after the air entrance the aerosol is generated and induced into the aerosol channel. After around a meter the two main sampling points are situated. These provide the

necessary aerosol for ELPI+, SMPS and the *Impinger*. The distance between both sampling points were chosen to enable isokinectic sampling, which means that the aerosol velocity inside the sampling tube is the same as the aerosol velocity of the aerosol flow through the channel, and to prevent any cross influences. The remaining aerosol is discharged into a cartridge filter.

In picture 2.1.1 two sampling points are situated before and after the *Impinger*, to measure crude and clean gas.

The aerosol test device is monitored by mass flowmeters, which regulate the pumping power to a set level. Furthermore the particle flow is monitored by a scanning mobility particle sizer (SMPS). Both systems receive real time data and are able to visualize the data every few seconds. The mass flowmeters are located at the bottom of the device, implemented in front of the orifice to the cylindrical cartridges. The SMPS is located at the second level of the aerosol test device.

At the left side of the aerosol test device the *Impingers* are located. These flasks are used to gather varying particles into different fluids, such as water or saline puffers.

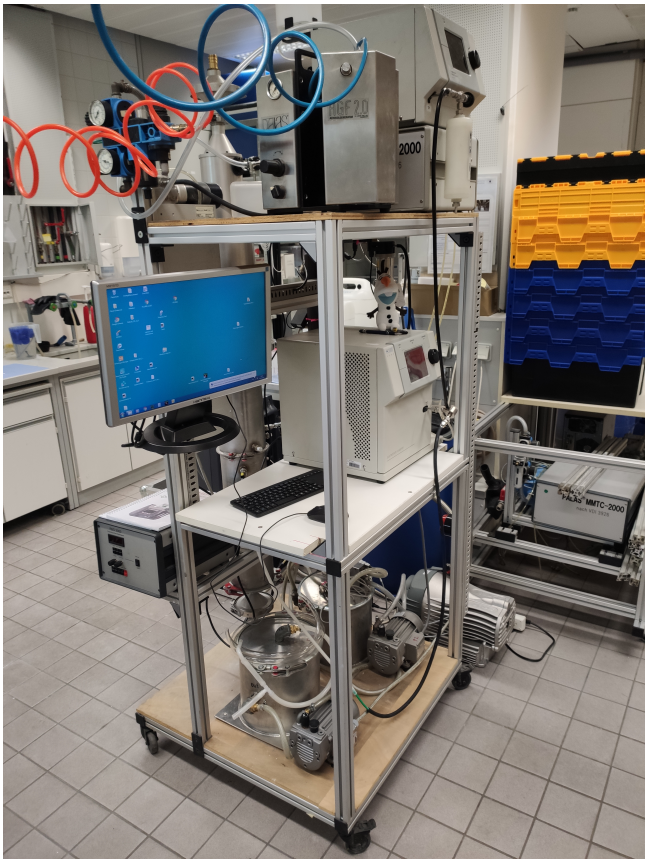

Figure 2.1.2: aerosol test device

Figure 2.1.2 shows a picture of the aerosol test rig. At the bottom of the picture the pumps are located. The middle stage houses the main controlling and data saving unit and the SMPS without the CPC. At the top of the device one aerosol generator is visible and in the back CPC got his place.

2.2 System parts

2.2.1 Aerosol channel

The aerosol channel is 1745 mm long and 24 cm in diameter and is fixed in vertical position. The main air is sucked in through an inlet situated on top of the aerosol channel. Right after the orifice is an absolute filter installed to prevent any airborne particles from ambient air to enter the device. The entrance for the test particles,

coming from the aerosol generator, is located 180 mm after the orifice. The aerosol generator and the aerosol channel is connected with synthetic tubes.

600 mm further down the channel the probe points are located, the first one leading to the SMPS and to the *Impingers*. The second one is connecting the aerosol channel with a secondary analysing device, mainly a electrical low pressure impactor (ELPI+).

At the bottom of the aerosol test device the main aerosol flow is discarded into a cylindrical cartridge. The opening leading to the cartridge is equipped with a mass flowmeter, which is supplying the necessary data to control the pumping power to ensure a stable and constant volume flow throughout the test rig.

2.2.2 Aerosol Generator

The aerosol generator used for high particle concentrations is the RBG 2000 from Palas- GmbH, it can provide an aerosol flow from 1 to 560 grams per hour. The RBG 2000 is an aerosol generator for non- cohesive particles. The generator consists of a solid material reservoir, dispersing head, dispersing cover and a precision brush. The reservoir is filled with the desired dust, than compressed with a tamper and convoyed to the precision brush. The rate at which the dust will be dispersed is precisely adjustable. In addition compressed air is used to transport the particles from the brush into the aerosol channel. The RBG 2000 aerosol generator is shown in figure 2.2.1. [2]

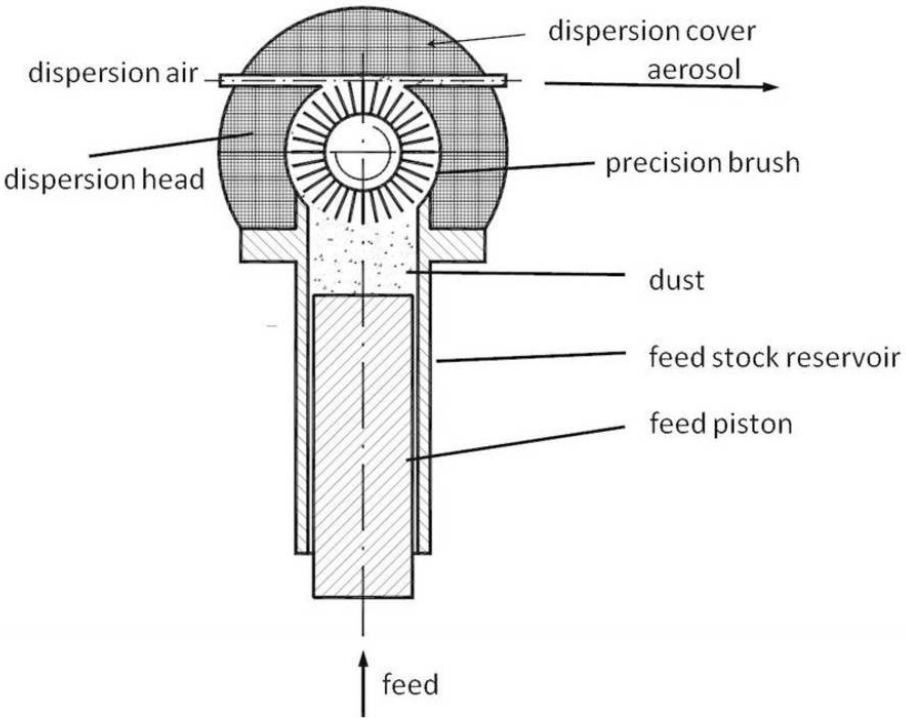

Figure 2.2.1: RBG schematic diagram [2]

The aerosol generator used for low particle concentration is the Palas AGF 2.0. The AGF 2.0 is an aerosol generator for the atomization of liquids and latex suspensions with a constant particle rate and defined particle spectrum. The generator consists of an liquid reservoir, a cyclone, which removes large particles out of the main aerosol flow, an orifice and a connection for compressed air. The Palas AGF 2.0 proides a volume flow form 6 to 17 l/min and an aerosol flow of 4g/h. [29]

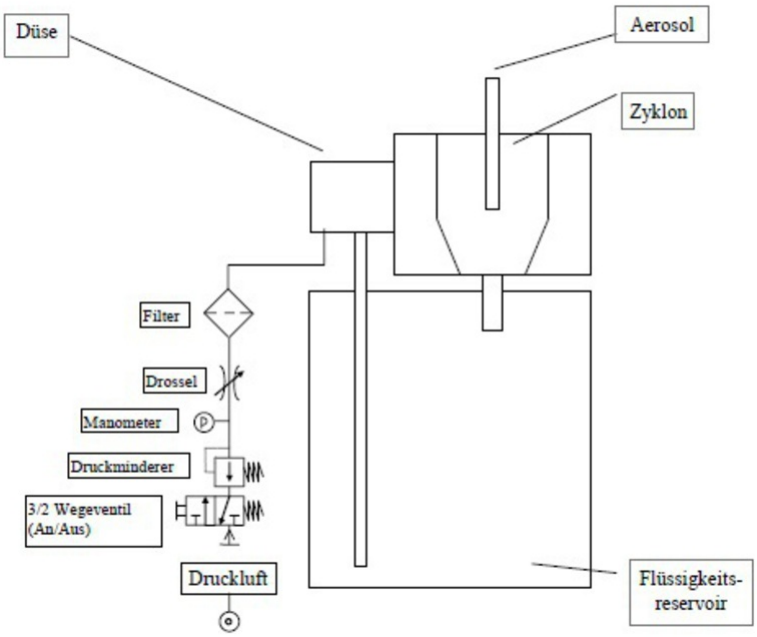

Figure 2.2.2: Palas AGF 2.0 schematic diagram [29]

Figure 2.2.2 shows the main parts of the Palas AGF 2.0. The aerosol is dispersed with compressed air, describe as *Druckluft*, the Laskin nozzle is described as *Düse*, the suspended particles are contained in the liquid reservoir, described as *Flüssigkeitsreservoir* and the cyclone, which separates big particles from the main aerosol flow is described as *Zyklon*.

2.2.3 Impingers

The *Impinger* is a washing bottle, used to gather airborne particles and force them into a liquid. The aerosol travels through a dip tube, the end of which is submerged in a solvent. Hence the particles in the airflow are forcefully bubbled through the liquid, increasing the chance of fixing particles in the fluid. Furthermore the *Impinger* is filled with vitreous bodies to drastically increase the collection efficiency. This idea was adopted from the paper *Collection efficiency of a midget impinger for nanoparticles in the range of 3 to 100 nm.*[37]

A schematic illustration is shown in figure 2.2.3. The scheme of the *Impinger*

shows the aerosol flow entering the system in a long tube, leading to the liquid medium and the vitreous bodies inside. The aerosol passes through the solvent and exits the flask through an outlet. The liquid medium linked with the glass bodies should enhance the probability of impaction of the particles with the medium, hence the collection efficiency rises.

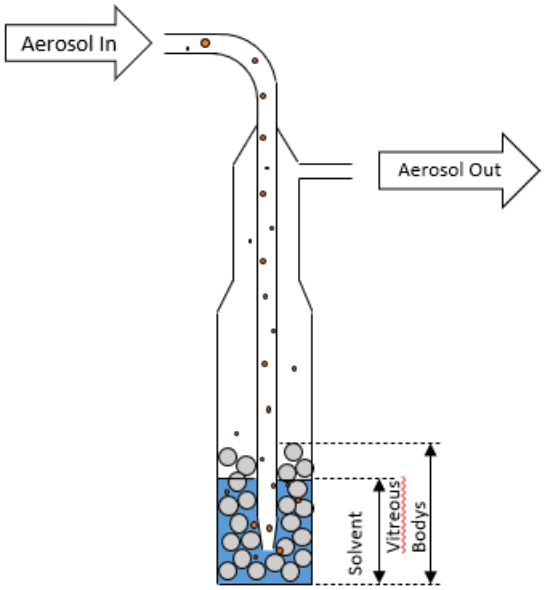

Figure 2.2.3: Scheme of the *Impinger* with Liquid and Beads

2.2.4 Analysing Equipment

SMPS

Two analysers were put into use, for two different particle concentration levels. The main particle monitoring device is the TSI 3080 electrostatic classifier, which is part of the scanning mobility particle sizer (SMPS). This SMPS consists of a differential mobility analyser (DMA) and a condensation particle counter (CPC). The system draws at a constant flowrate, aerosol out of the main channel and provides data, regarding number and size of the tested particle sample. The TSI 3080 is able to analyse particles ranging from 10 to 1000 nm. [33]

ELPI

The second analyser is the electrical low pressure impactor (ELPI+) from Dekati. This instrument is able to provide real time data on particle number, active surface, mass concentration and size distribution.

The aerosol is introduced into a unipolar diffusion charger which is based on needle type corona discharge.[21] After the corona discharge, the remaining ions are removed from the aerosol flow by a ion trap. The aerosol than enters the impactor stages, starting with a pre- separator stage to get rid of large particles and followed by 13 impactor stages. The last impactor stage is a filter, which gathers the particles that were to small to deposit inside the preceding impactor stages. The last stage is connected to a electrometer, hence a signal is retrieved from the smallest particle fraction. The ELPI+ is able to measure particles from 6nm to 10 µm. The impactor stages run at a pressure of around 40 mbar, the vacuum is provided by an external pump.

2.2.5 Pumps

The aerosol test device needs two pumps. The main air flow through the channel is provided by a Becker rotary vane vacuum pump, with the identification number VT 4.8. The pump has an inlet capacity up to 8,7 m^3/h. The pump is exhibited ins figure 2.2.4.

The second pump feeds the *Impingers* and the SMPS and is a Ehrler & Beck rotary vane vacuum pump with the identification number VT 4.4. The pump has an inlet capacity of 4 m^3/h.

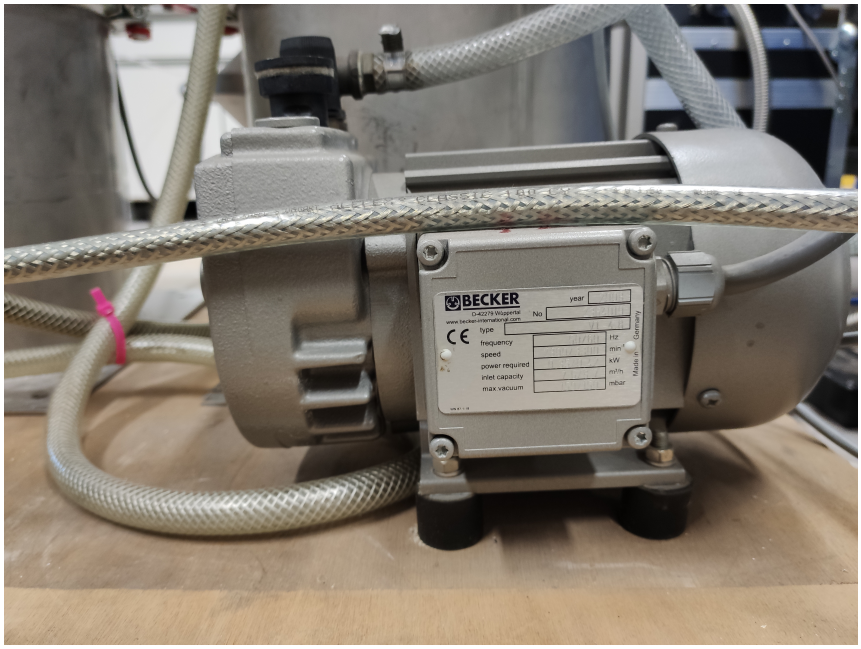

Figure 2.2.4: Becker Pump, Main Pump (Pump 2)

Two cylindrical cartridges prevent the aerosol particles to enter the pumps, therefore the main flow is close to particle free before entering the pumps. This two cartridge filters are necessary, because the aerosol particles severely damage the pumps, if not separated beforehand.

2.3 Controlling and Monitoring

2.3.1 Measuring Board

To control and monitor the airflow and the pumping power level, a measuring board from Meilhaus typ Redlab 1208LS is utilised. The card possesses analogue and digital entrances and exits and is connected via USB- wire to the PC. The measuring board is presented in figure 2.3.1.

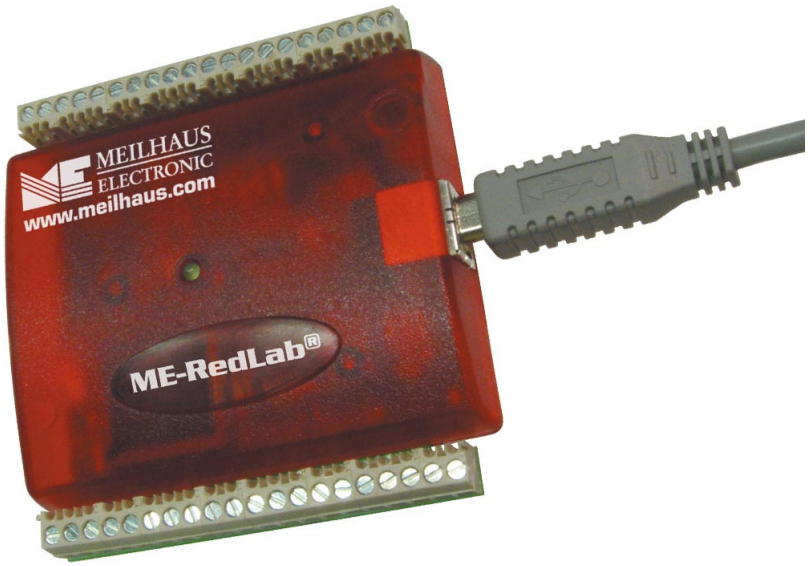

Figure 2.3.1: Meilhaus Redlab 1208LS [1]

2.3.2 Software

Lab View National Instruments 2019 [3] is used to control and monitor the aerosol test device and collect and safe the data retrieved from the instruments. Furthermore the software enables the manual control of the aerosol test device. The user interface is presented in figure 2.3.2.

The software interface shows two tabs, the first one *Seite 1* is the selection of the data path. the second one *Seite 2* is monitoring and operating interface. The interfaces allows to control the power level of the two pumps and provides information of the set level and the actual power level. The pump data is visualized during the measurements on the interface in the right top corner. Furthermore time and pressure difference before and after the cylindrical cartridge filter are collected and showed.

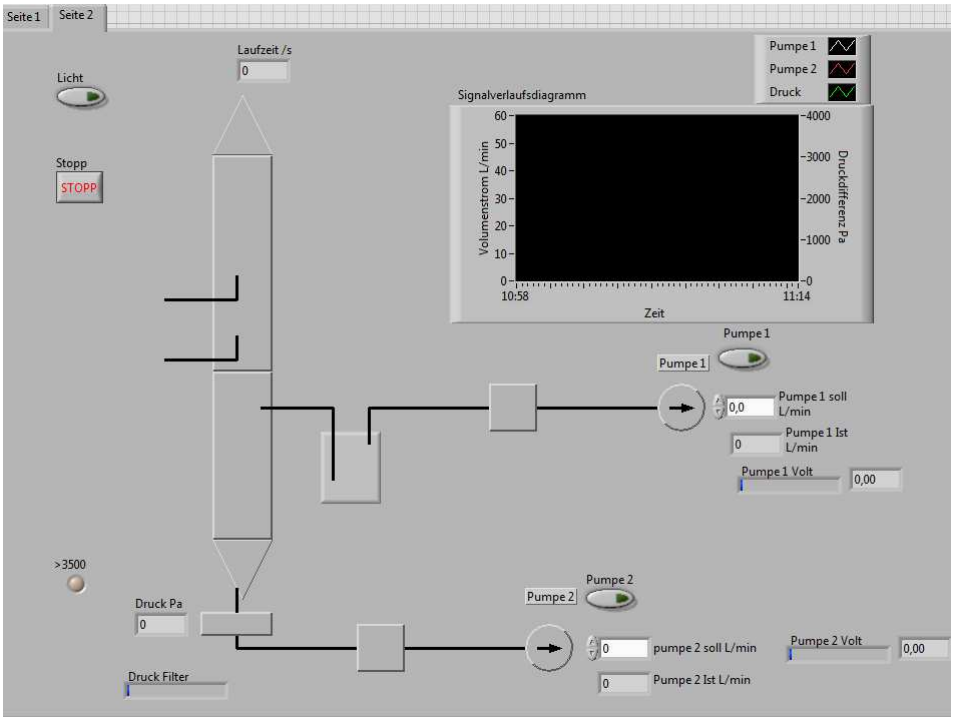

Figure 2.3.2: User Interface of the controlling software

3 Experimental

Now that the aerosol measurement device is operational, some test runs have to be conducted to assure that the device is running correctly. Furthermore it is necessary to calibrate the pumps and the analysing equipment and adjust the flowrates to an optimum level. Therefore a sufficient available test dust is used, which is Titanium dioxide bulk material. The bulk material is characterised by the on site TSI 3080, the Malvern Mastersizer 2000[19] and the Anton Paar Litesizer 500[7].

3.1 Production of a stable aerosol flow with the Palas AGF 2.0

The first experiment conducted with the newly built aerosol test device, is the production of a stable aerosol flow with the Palas AFG 2.0, the operating scheme is depicted in figure 2.2.2. This experiment should show, that the aerosol generators and the aerosol test device need time to produce a stable aerosol flow. The course of the measurement is monitored by the devices software and examined by the ELPI+. The ELPI+ measures a sample every 15 seconds, therefore a visualization of the course of the measurement is possible.

Three substances are used as test dusts for this experiment, titanium dioxide, silicon dioxide and zinc oxide, all provided by the Joint Research Center of the European Union, short JRC. The powder is a representative nanomaterial.

The experiment preparation starts with the weigh- in of the dust sample. Afterwards a certain amount of distilled water is mingled with the dust material and stirred till an homogenous suspension is established to obtain a particle concentration of 10 mg dust sample per 100 ml distilled water. The suspension is transferred to the Palas AGF 2.0 reservoir and the aerosol generator is connected

to the compressed air. Meanwhile the aerosol test device is started to allow the flow, generated by the main pumps 1 & 2 to become stationary.

3.1.1 Titanium Dioxide

The preparation starts with the weigh in of the dust material. 5 mg of Titanium dioxide from the European Commission Joint research centre were weight in and 50 ml of distilled water were added to the powder and stirred well. Then the suspension was transferred to the aerosol generator as describe at the beginning of the section. The pumps worked throughout the whole measurement at a set level, Pump 1 ran at seven litres per minute and Pump 2 ran at 30 litres per minute.

The ELPI+ conducted fifteen ambient air measurements and 244 aerosol samples. The whole run time was 1 hour 6 min and 15 sec.

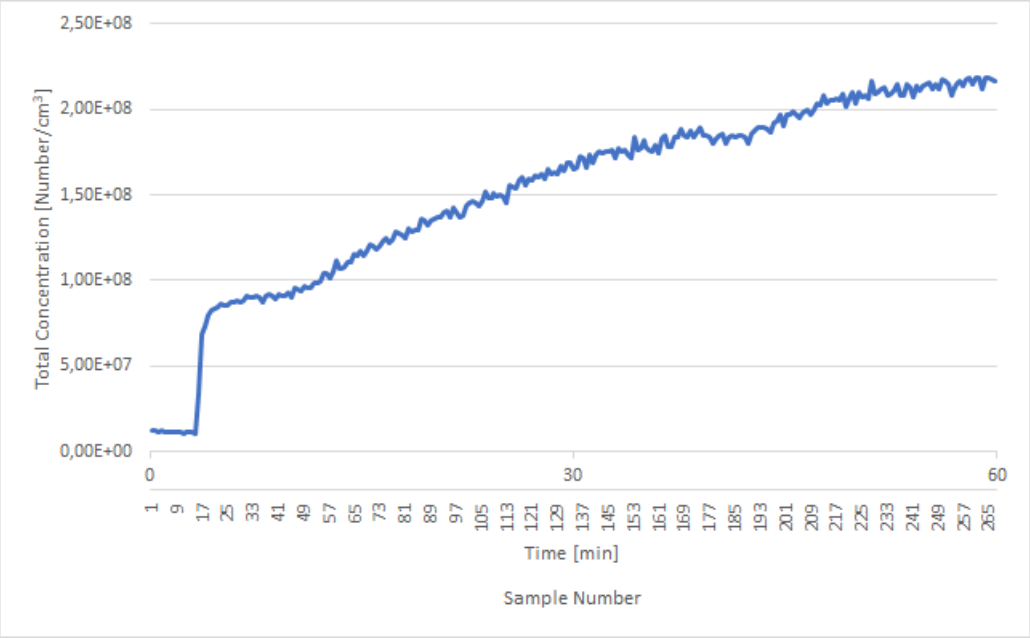

Figure 3.1.1: ELPI: Total concentration over time and sample, TiO_2

Figure 3.1.1 shows the total concentration per cubic centimetre of Titanium dioxide over time and sample number as seen by the ELPI+. Total concentration means the sum of all the stages.[22] The ambient samples starts with sample 1 to 15. Then two samples 16 and 17 are in the transition region from ambient air to

aerosol flow. The particle concentration increases by the factor 9 in 30 seconds or two samples.

The total particle concentration rises over the course of the measurement, but flattens towards the end of the measurement. After 45 to 50 min the aerosol flow does not differ much from the preceding samples, it is therefore stable.

Possible explanation for this phenomenon is the sedimentation of particles. The aerosol generator Palas AGF 2.0 draws the suspension of titanium dioxide and distilled water out of a liquid reservoir via a long synthetic tube, which is situated at the bottom of the flask. Therefore the concentration of particles rises over the course of the measurement, due to the sedimentation of titanium dioxide particles.

3.1.2 Silicon Dioxide

The preparation starts with the weigh in of the dust material. 7,5 mg of Silicon dioxide from the European Commission Joint research centre were weight in and 75 ml of distilled water were added to the powder and stirred well. Then the suspension was transferred to the aerosol generator as describe at the beginning of the section. The pumps worked throughout the whole measurement at a set level, Pump 1 ran at seven litres per minute and Pump 2 ran at 30 litres per minute.

The ELPI conducted no ambient air measurements, due to a valve problem, but the aerosol measurements worked without any difficulties. Therefore 409 aerosol samples were retrieved. The total runtime for this experiment was 1 hour, 42 minutes and 15 seconds.

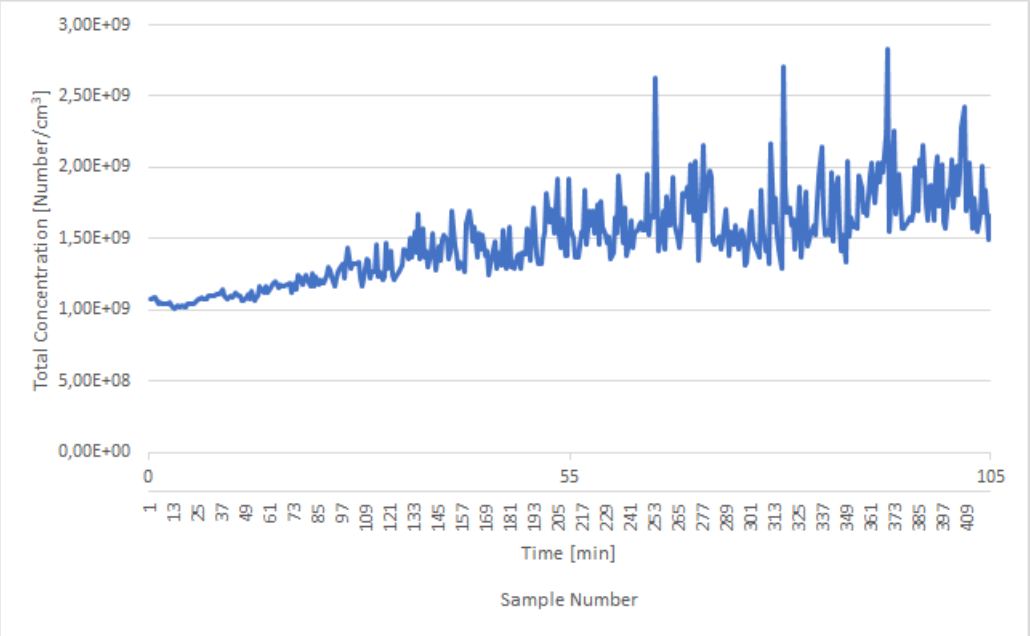

Figure 3.1.2: ELPI: Total concentration over time and sample, SiO_2

Figure 3.1.2 shows the total concentration of Silicon dioxide over time and sample number. All samples are aerosol measurements.

The trend towards higher total particle concentrations is visible in figure 3.1.2 but after 50 to 60 min the curve flattens out. But the ELPI+ depicts an unstable aerosol flow. Towards the end of the measurement the ELPI+ registered a few peaks of high total concentration.

3.1.3 Zinc Oxide

The preparation starts with the weigh in of the dust material. 8 mg of Zinc oxide from the European Commission Joint research centre were weight in and 80 ml of distilled water were added to the powder and stirred well. Then the suspension was transferred to the aerosol generator as describe at the beginning of the section. The pumps worked throughout the whole measurement at a set level, Pump 1 ran at seven litres per minute and Pump 2 ran at 30 litres per minute.

The ELPI+ conducted sixteen ambient air measurements and 253 aerosol samples. The total runtime was 1 hour 8 min and 15 sec.

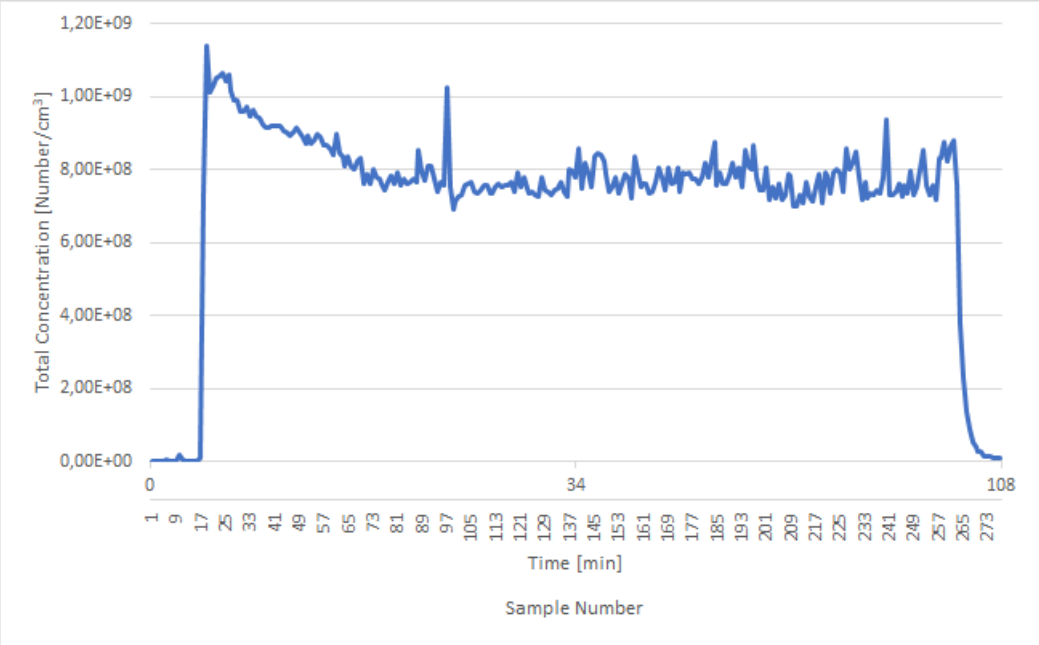

Figure 3.1.3: ELPI: Total concentration over time and sample, ZnO

Figure 3.1.3 shows the total concentration of zinc oxide over time and sample number as observed by the ELPI+. The diagram presents a beautiful course of a whole measurement, clearly visible the points, where the aerosol generator has been turned on, sample 17 and off, sample 263.

The highest total particle concentration is found right after the aerosol generator was switched on. The concentration slowly decreases over the course of the measurement. After 20 minutes the flow is stable till the end of the measurement.

3.2 Presentation of the Particle Sizes

In this part of the thesis, the data retrieved from the first experiment is visualized and shortly discussed. Both ELPI+ and SMPS are presented and their findings are put into charts to see, the observation of each analyser.

To receive a coherent image of the aerosol in the channel, both analysers start their measurements at the same time. But the SMPS needs sixty seconds for one measurement and fifteen seconds for adjusting to next run, thus needing seventy five seconds in total for a full measurement. Meanwhile ELPI+ conducts one full

measurement in fifteen seconds and starts right away with the next one. Therefore the ELPI+ receives five samples, while the SMPS receives only one sample in the same time spawn.

The ELPI+ has a resolution of fourteen channels, ranging from 6 to 6800 nm.

The SMPS uses for this measurements 99 channels ranging from 15,7 to 532,8 nm.

3.2.1 Titanium Dioxide

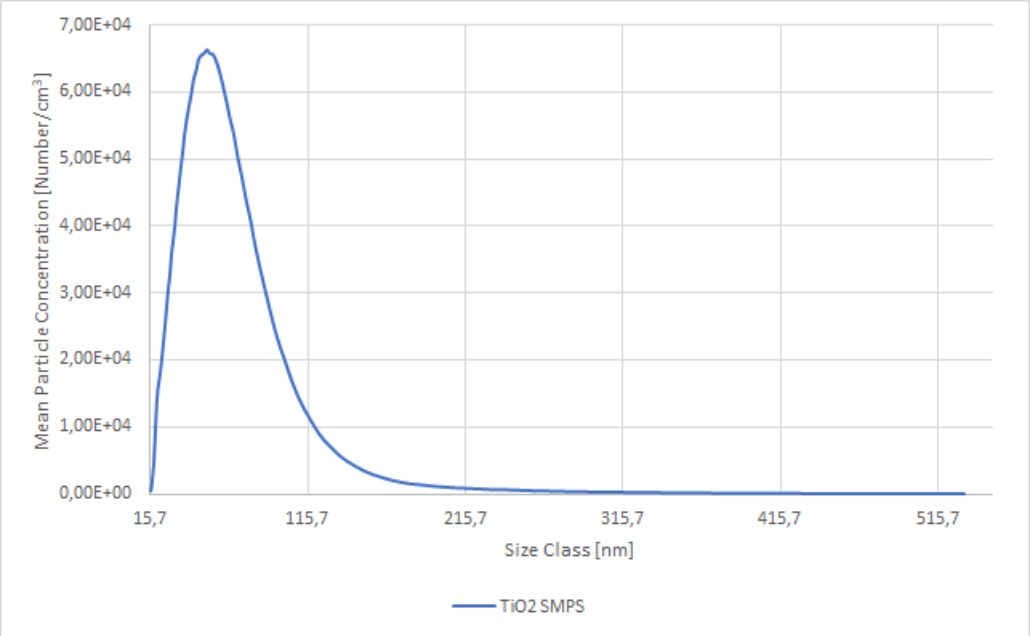

Figure 3.2.1: SMPS: Mean Particle Concentration of the Aerosol, TiO_2

Figure 3.2.1 shows the course of the mean particle concentration of the stable aerosol over size class of titanium dioxide as observed by the SMPS. The SMPS observes the highest mean particle concentration in the size class ranging from 51,4 to 53,3 nm. Furthermore most of the particles present in the JRC sample have a Stokes diameter from less than 100 nm.

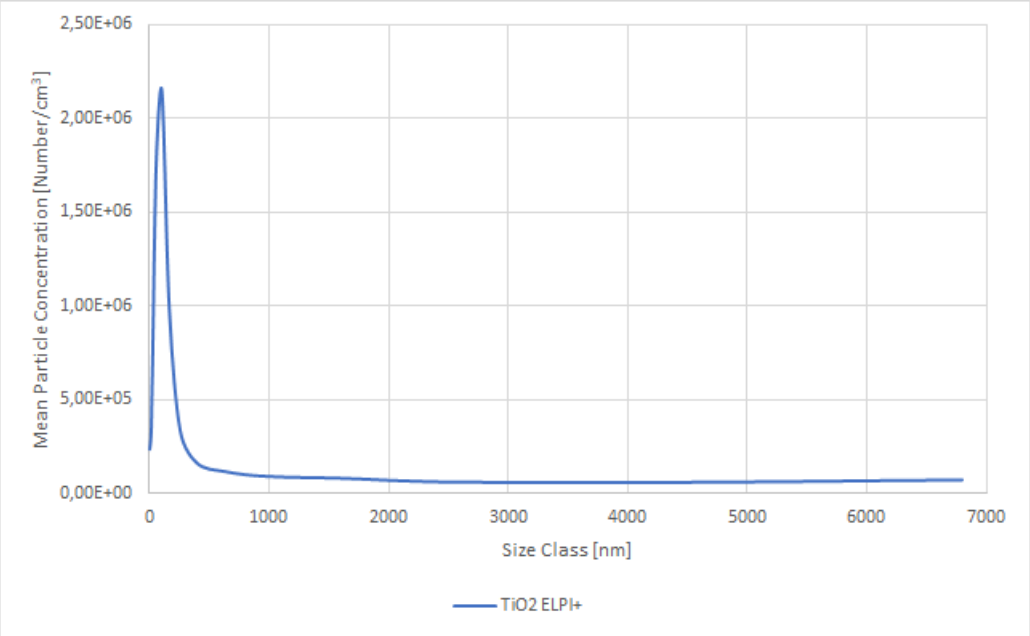

Figure 3.2.2: ELPI: Mean Particle Concentration of the Aerosol, TiO_2

Figure 3.2.2 shows the course of the mean particle concentration of the stable aerosol over the size class of titanium dioxide as observed by the ELPI+. The ELPI+ finds the highest mean particle concentration between the channels 60 to 108 nm.

3.2.2 Silicon Dioxide

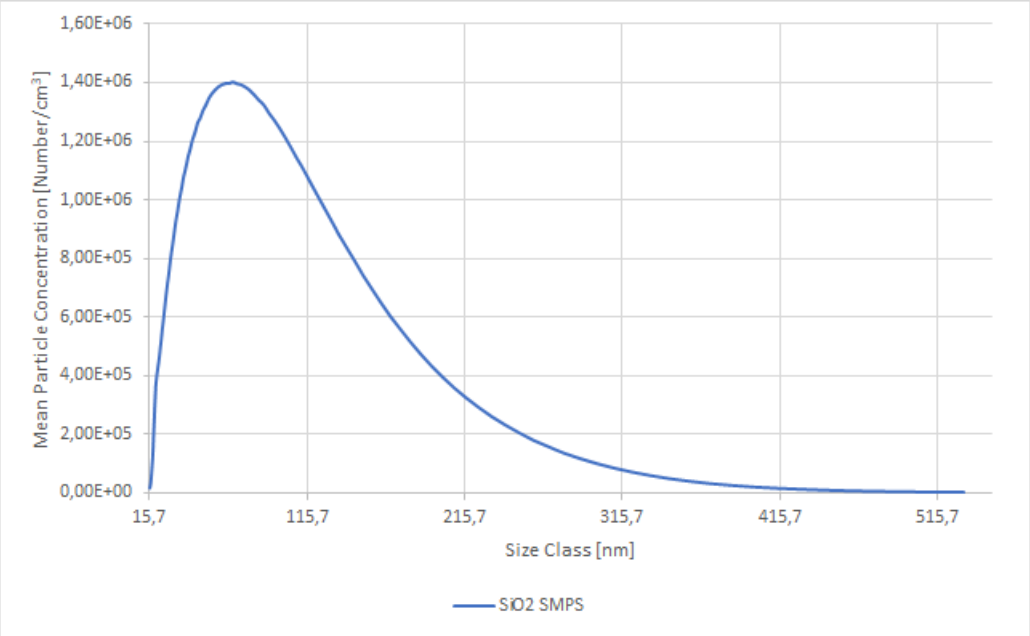

Figure 3.2.3: SMPS: Mean Particle Concentration of the Aerosol, SiO_2

Figure 3.2.3 shows the mean particle concentration of the stable aerosol over size class of silicon dioxide as seen by the SMPS. Other than the titanium dioxide sample, the highest value is retrieved from the channel 68,5 to 71 nm. In addition the SMPS records high mean particle concentrations for greater particles, compared to the titanium oxide sample.

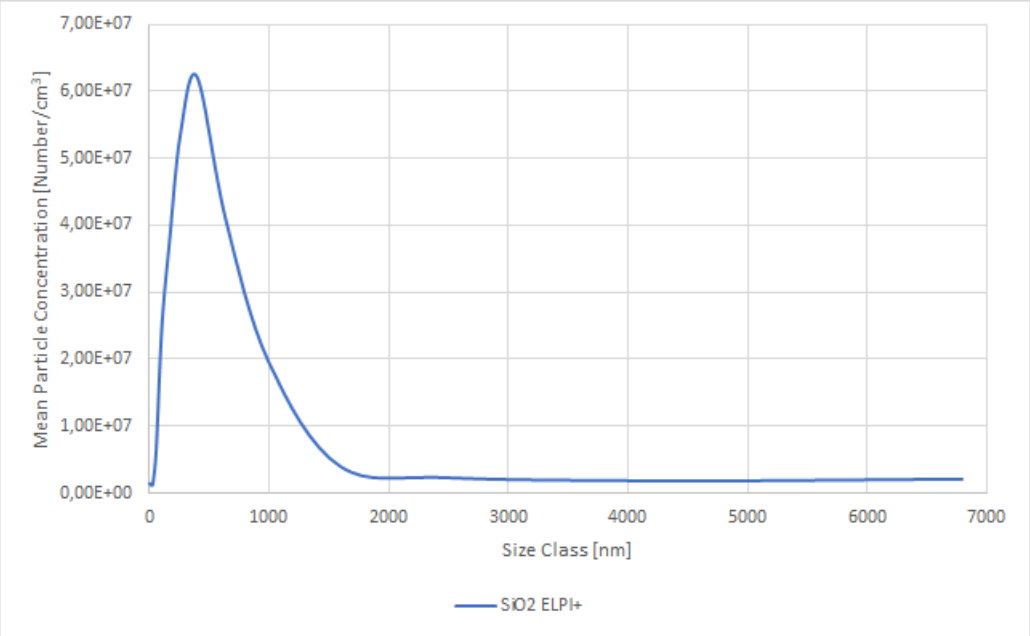

Figure 3.2.4: ELPI: Mean Particle Concentration, SiO_2

Figure 3.2.4 shows the course of the mean particle concentration of the stable aerosol over size class of silicon dioxide as observed by the ELPI+. The ELPI+ retrieves the highest mean particle concentration value from the channel ranging from 400 to 640 nm.

3.2.3 Zinc Oxide

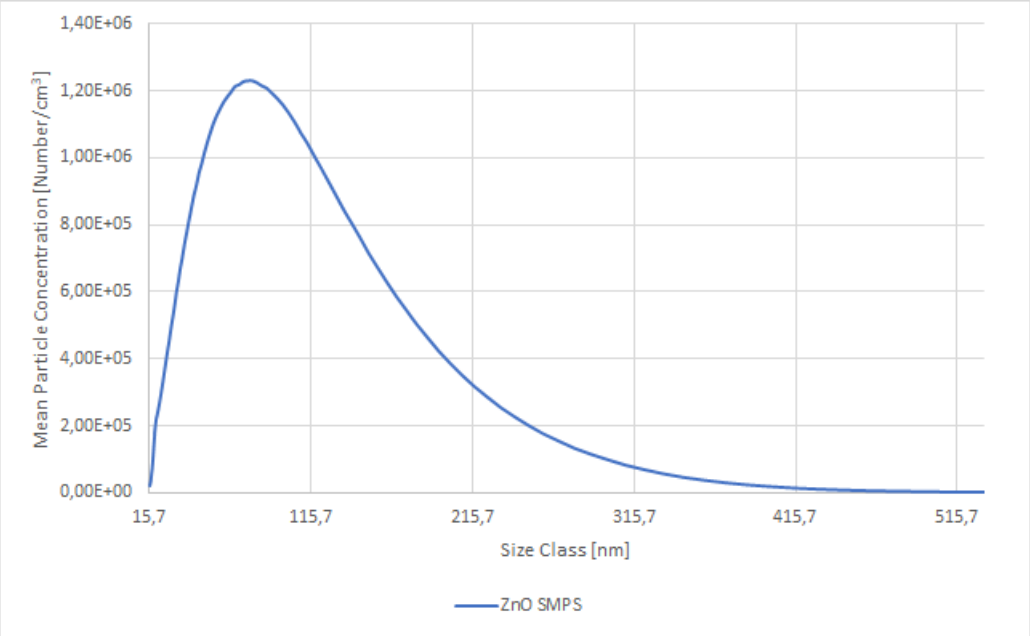

Figure 3.2.5: SMPS: Mean Particle Concentration of the Aerosol, ZnO

Figure 3.2.5 shows the course of the mean particle concentration of the stable aerosol over size class of zinc oxide as observed by the SMPS. The SMPS observes the highest mean particle concentration in the size class ranging from 79,1 to 82 nm. The curve shares lots of resemblance to the silicon dioxide curve.

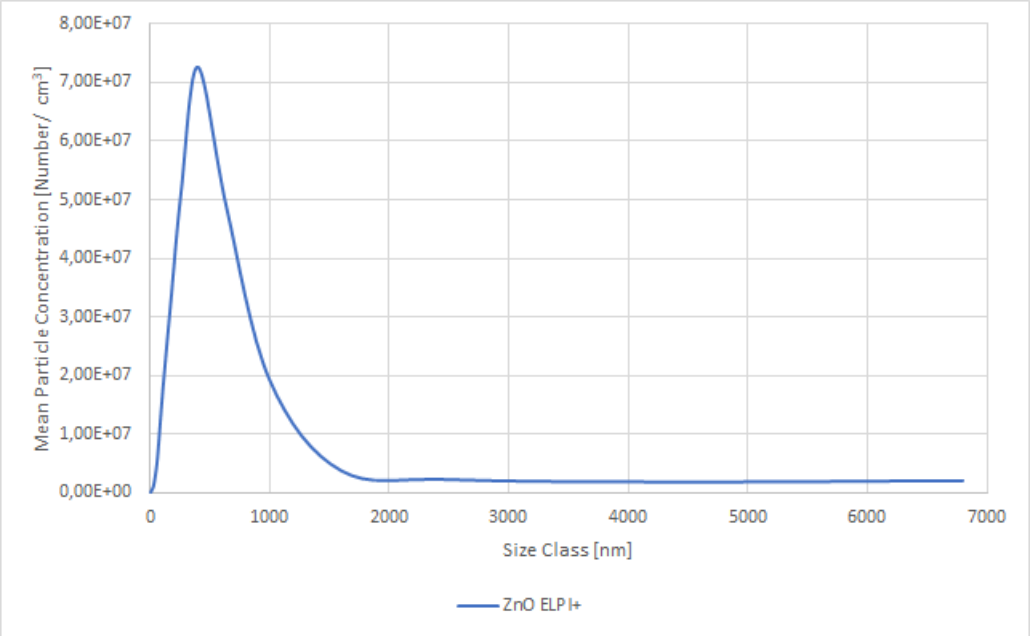

Figure 3.2.6: ELPI: Mean Particle Concentration of the Aerosol, ZnO

Figure 3.2.6 shows the course of the mean particle concentration of the stable aerosol over size class of zinc oxide as observed by the ELPI+. The ELPI+ retrieves the highest mean particle concentration value from the channel ranging from 400 to 640 nm.

3.3 Collection efficiency

This experiment runs at a high level particle concentration. Therefore the ELPI+ is not able to parallelly measure, due to the risk of damaging the equipment with such high particle concentrations.

The first step to start the aerosol measurement device is to turn on the energy supply. Afterwards start the PC and the software to control the pumps and the SMPS. If everything launched correctly the pumps will start their duty. After a few moments a constant airflow through the whole device should be visible on screen. The desired dust is weighed in the dust reservoir of the aerosol generator and compressed with the tamper. Furthermore the filling level of the reservoir is manually measured. The filling height limits the time at which the aerosol

generator can hold up a certain feed rate.

After the dust reservoir is put into place the measurement of the ambient air is started. To zone out the common airborne particles from the test dust, a few minutes prior to the initiation of the aerosol generator the SMPS already measures the airflow through the device. The next step is to switch on the aerosol generator. After a few seconds a tremendous rise in airborne particles should be visible on the SMPS software surface. The rise will flatten out when a stationary aerosol flow is established.

After the desired circles of measurements, the aerosol flow is connected to the *Impinger* and the SMPS is connected to the outlet of the wash flask. The needed data regarding the collection efficiency is monitored and saved.

Afterwards the aerosol generator is switched off but the SMPS measurement continues till the same level of ambient particle concentration is reached. However it is possible that, due to external parameters, such as an open doors, open windows, or leakage of the aerosol measurement device the starting level can not be reached for the moment.

The collection efficiency was measured for three different materials, titanium dioxide, silicon dixode and zinc oxide.

For this purpose the flask was filled with 20 ml of phosphate- buffered saline (PBS) and the tube connecting the aerosol channel to the *Impingers* were submerged into the liquid.

PBS was used instead of distilled water, due to the potentially further use of the gathered particles, because PBS is commonly used for biological and medical applications.

At first the aerosol flow is measured by the SMPS. After a few measurements the aerosol flow is connected to the *Impinger* flask and the particle stream is travelling first through the liquid inside the flask, than going into SMPS to measure the residue particles. The idea is that the particles interact with the liquid, either via impaction or diffusion, and should be tied to the solvent. This reduction in particles after the *Impinger* is visible.

3.3.1 Titanium Dioxide

The measurement preparation started with the weight in of the JRC titanium dioxide dust sample. 10,557 g of TiO_2 were filed in the dust reservoir and tampered to the filling height of 28,6 mm.

Pump 1 was set to the level of 30 litres per minute and pump 2 was set to 7 litres per minute. The SMPS measured two crude gas samples and 31 clean gas samples.

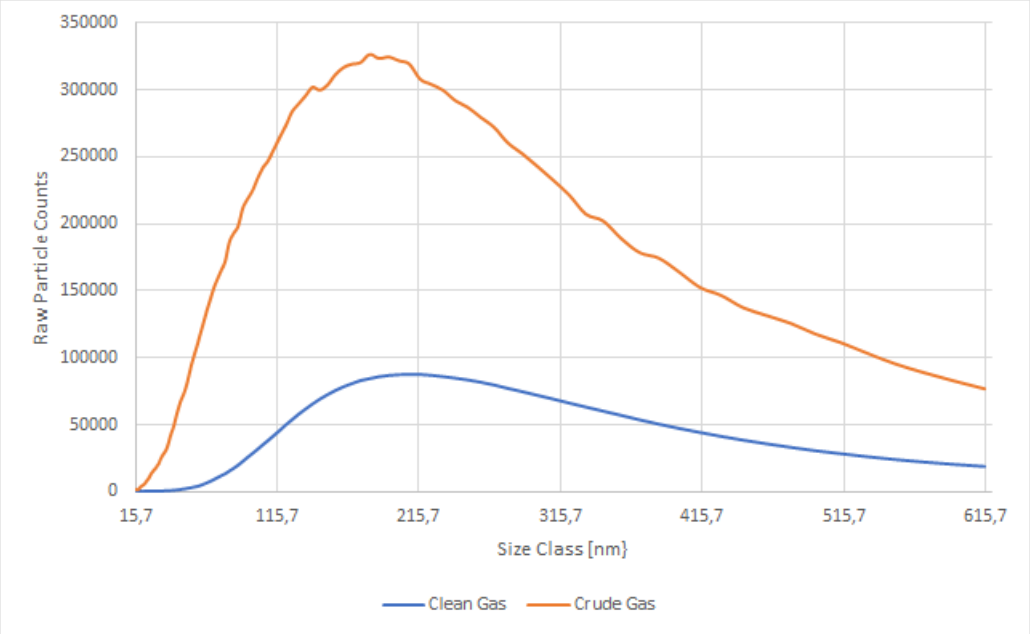

Figure 3.3.1: Course of the Measurement, TiO_2

Figure 3.3.1 shows the course of the titanium dioxide measurement. The two curves depict the number of counted particles over their size class, the orange curve presents the crude aerosol and the blue curve shows the reduction of particles after the aerosol travelled through the liquid medium.

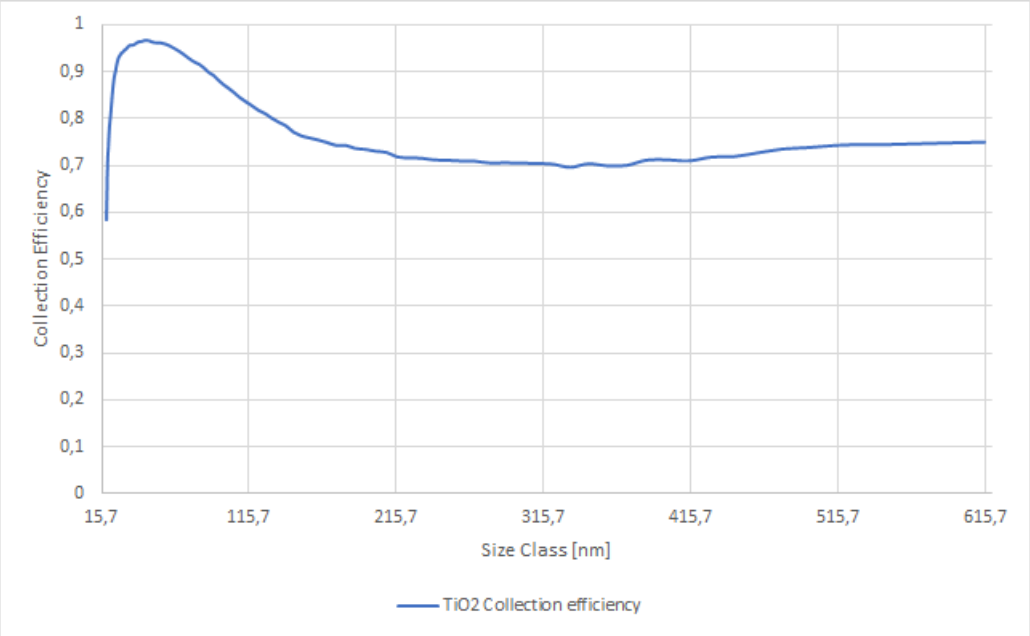

Figure 3.3.2: Collection Efficiency, TiO_2

Figure 3.3.2 depicts the course of the collection efficiency of the *Impinger* on titanium dioxide. The efficiency is not equally distributed over all size classes. Hence smaller particles ranging from 15,7 to 115,7 nm have a higher deposition affinity, than bigger particles.

3.3.2 Silicon Dioxide

The measurement preparation started with the weight in of the JRC silicon dioxide dust sample. 10,089 g of SiO_2 were filled in the dust reservoir and tampered to the filling height of 93,3 mm.

Pump 1 was set to the level of 30 litres per minute and pump 2 was set to 7 litres per minute. The SMPS measured four crude gas samples and 27 clean gas samples.

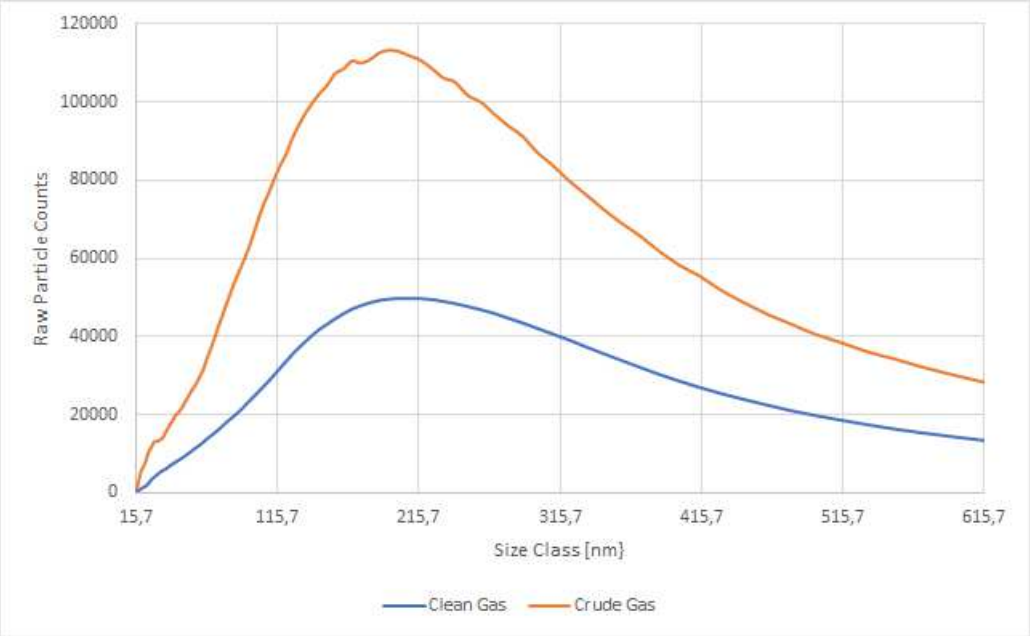

Figure 3.3.3: Course of measurement, SiO_2

Figure 3.3.3 shows the course of the silicon dioxide measurement. The curves have a similar appearance to the titanium dioxide measurement.

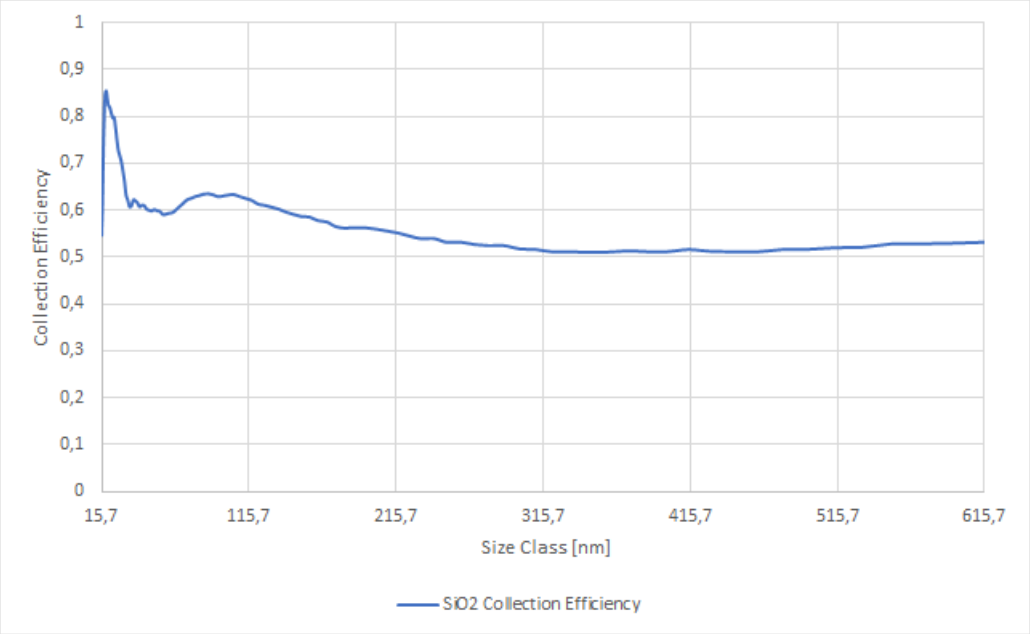

Figure 3.3.4: Collection Efficiency, SiO_2

Figure 3.3.4 shows the collection efficiency in regard of silicon dioxide. The curve is unsteady for smaller particles, ranging from 15,7 to 28,9 nm, but straightens out for the rest of the measurement at around 50% efficiency.

3.3.3 Zinc Oxide

The measurement preparation started with the weight in of the JRC zinc oxide dust sample. 10,000 g of ZnO were filed in the dust reservoir and tampered to the filling height of 42,0 mm.

Pump 1 was set to the level of 30 litres per minute and pump 2 was set to 7 litres per minute. The SMPS measured seven crude gas samples and 49 clean gas samples.

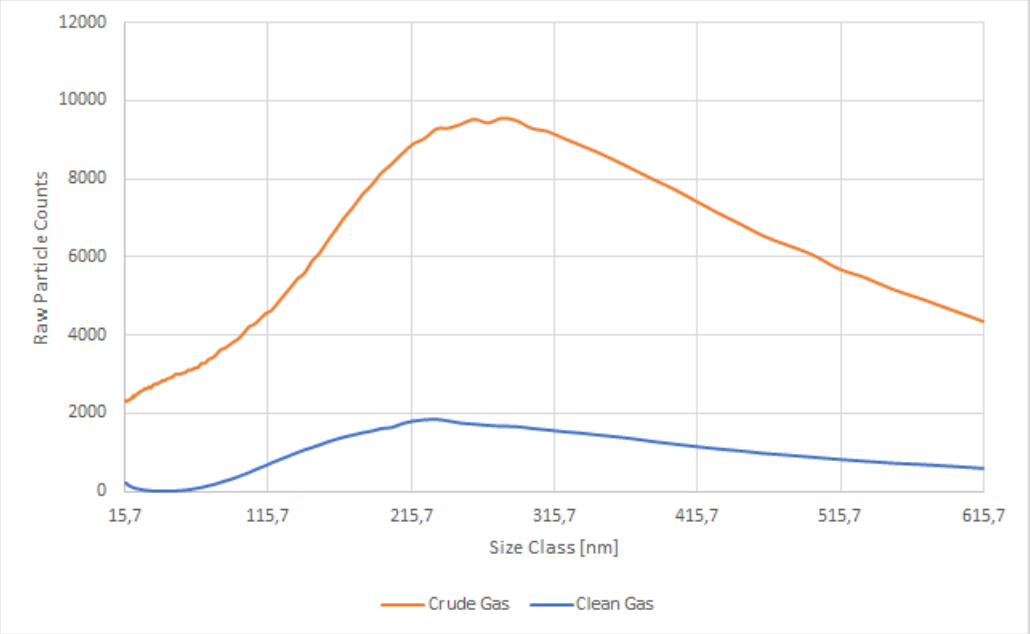

Figure 3.3.5: Course of the measurement, ZnO

Figure 3.3.5 shows the course of the measurement for zinc oxide. The chart 3.3.5 has a relative low raw particle count value, compared to the other two dust samples.

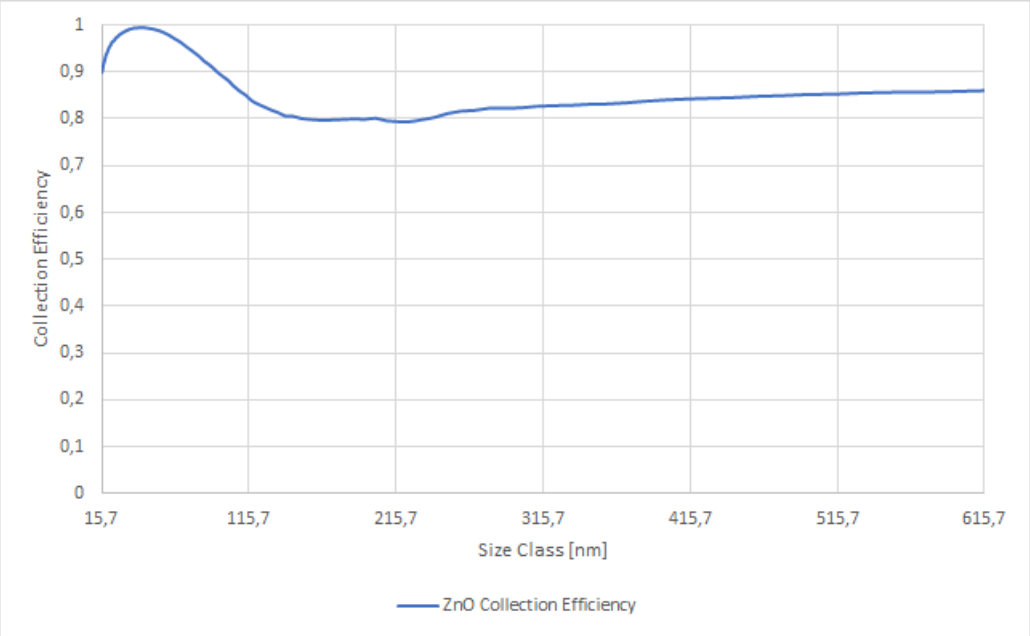

Figure 3.3.6: Collection Efficiency, ZnO

Figure 3.3.6 shows the collection efficiency of the *Impinger* with zinc oxide. The course of the curve is for smaller particle sizes, ranging from 15,7 to 59,4 nm close to one, therefore most of the particle are depositioned in the liquid medium of the washing flask. The collection efficiency decreases for bigger particle sizes, than 60 nm, but stabilises between 80% ti 85%.

4 Outcome and Discussion

The results and visualised data from the Experimental part of this thesis is discussed in detail in this chapter. Furthermore problems and difficulties, regarding the measurements and evaluation of the received data are addressed.

4.1 Setup and Mode of Operation Discussion

The aerosol test device was successfully built and tested and the device achieved all of the demanded requirements. Furthermore the production of a stable aerosol flow could be established and the outcome is presented in section 3.1.

The results show that the Palas AGF 2.0 needs some time to produce a constant aerosol flow and that the duration needed to do so is dependent on different factors, including material parameters. Furthermore the aerosol generator Palas AGF 2.0 is able to establish a constant aerosol flow after 45 to 50 minutes for titanium dioxide, depicted in figure 3.1.1, 50 to 60 minutes for silicon dioxide, depicted in figure 3.1.2 and 25 to 30 minutes for zinc oxide, depicted in figure 3.1.3.

A few problems rose with the stability of the aerosol, due to clogging of pipes and tubes and the sedimentation of particles inside the suspension reservoir of the Palas AGF 2.0. Although the physical dimensions of the aerosol test rig and especially the tube dimensions fit the requirements for particle concentrations, which were present during the experiments, clogging was a problem. To prevent any other occurrence, the clogged pipes, where thoroughly cleaned after every conducted experiment, yet the problem persisted. An appropriate remedy has not been found.

Regarding the sedimentation of particles, a stirring unit can solve this problem, but was not installed, due to the inaccessibility of the suspension reservoir.

4.1.1 Calculation of the size group factor

Comparing the ELPI+ with the SMPS is comparing aerodynamic particle diameter with Stokes particle diameter. The aerodynamic diameter is defined as a diameter of a unit density spherical particle having the same settling velocity as the actual particle. Another widely used definition is the Stokes diameter, which is the diameter of a spherical particle having the same bulk density and settling velocity as the actual particle.[22]

According to Maricq et al. paper [23] three major complication occur, when comparing the ELPI+ to the SMPS.

The first one being the difference between aerodynamic and Stokes diameter.

The second complication concerns the need to correct the currents on the upper, large particle, impactor stages for small particle losses that occur as the aerosol passes through. The losses occur both because of diffusion and electrostatic forces experienced by the particles. An empirical correction algorithm is employed by the ELPI software to account for the stage by stage losses. The corrections can be significant for the first few stages in the original impactor design, due to charging of the teflon used to insulate between stages. [23]

Particle bounce presents a third difficulty, since it transfers charge from one stage to another stage that is meant for smaller particles.[23] Thus falsifying measurements and shifting particle concentration further down the stages.

These findings should be kept in mind by the dear reader of this thesis.

The data retrieved by SMPS and the ELPI+ seems to differ greatly, if the size classes are compared and I wanted to know how great the difference in the respective size class is.

To find a correlation between the ELPI+ and the SMPS size groups, some calculations were conducted. The retrieved analyser data is divided into equal long lasting time frames, which means a certain number of samples that were taken at the same time by the ELPI+ and SMPS. The number of samples in such a time frame is dependent on the number of samples that each analyser made during this period. The duration of each time frames varies from substance to substance. Hence for one substances, e.g. Titanium dioxide, the time frame and resulting number of samples stays the same for the whole calculation.

The time frames are paired up with the same time frame from the other analyser and put into diagram, resulting in a scatter plot. To make things more clear, the procedure and outcome of this calculation is further explained based on the titanium dioxide results.

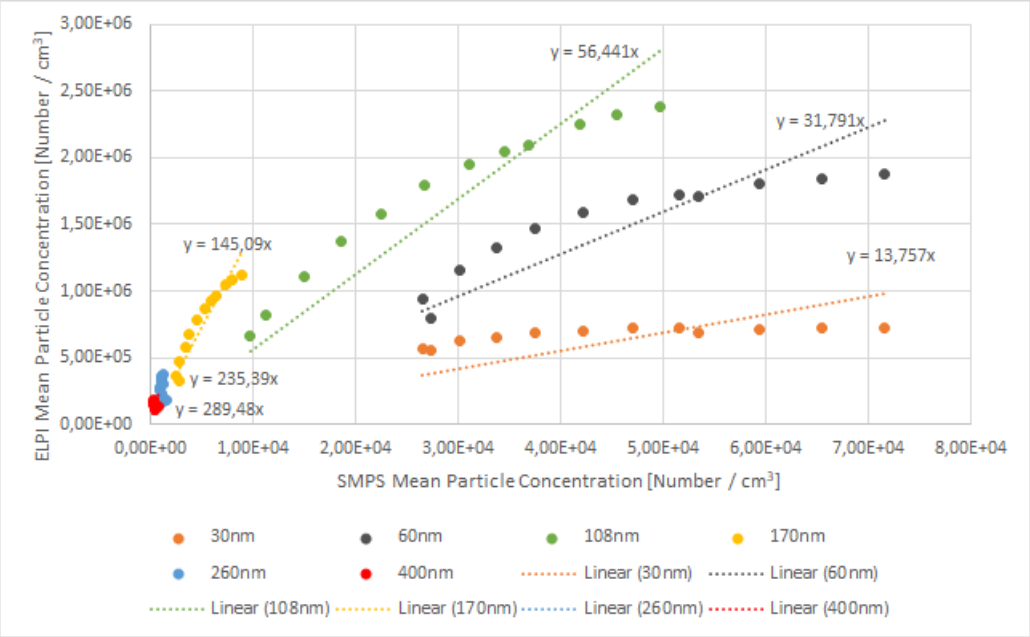

Figure 4.1.1: Correlation factors for TiO_2

Figure 4.1.1 shows on the abscissa the number concentration of the SMPS measurements, the ordinate shows the number concentration of the ELPI+ measurements. Each dot represents a time frame of four consecutive measurements by the SMPS, respectively twenty consecutive measurements by the ELPI+ or 5 minutes of sampling time. Twelve time frames per size group were calculated for titanium dioxide.

The calculation for size class coefficient was done via linear regression. The regression line starts at the origin of the Cartesian coordinate system and is calculated for each size group. The value of correlation factor is depicted as the number value of the x variable close to the linear equation in the scatter diagrams.

The chart shows that for smaller particles the ELPI+ and the SMPS retrieve similar results, differing in the dimension of $1,3 * 10^1$ to $5,6 * 10^1$. But the larger the particles get, the correlation starts to decrease, resulting in a factor of around

300 for the largest size group ranging from 260 to 400 nm.

Furthermore the rise of concentration over course of the measurement is visible, but not equally distributed between SMPS and ELPI+. At the 30 nm size group the SMPS observes a far greater growth than the ELPI+, but at greater particle size class this phenomena seems to be reversed. At 170 nm the ELPI+ observes a rise in particle concentration, which in turn the SMPS does not measure. The discrepancy in value is the highest at the largest size group at 400 nm, but the accuracy of both analyser seems to be equal.

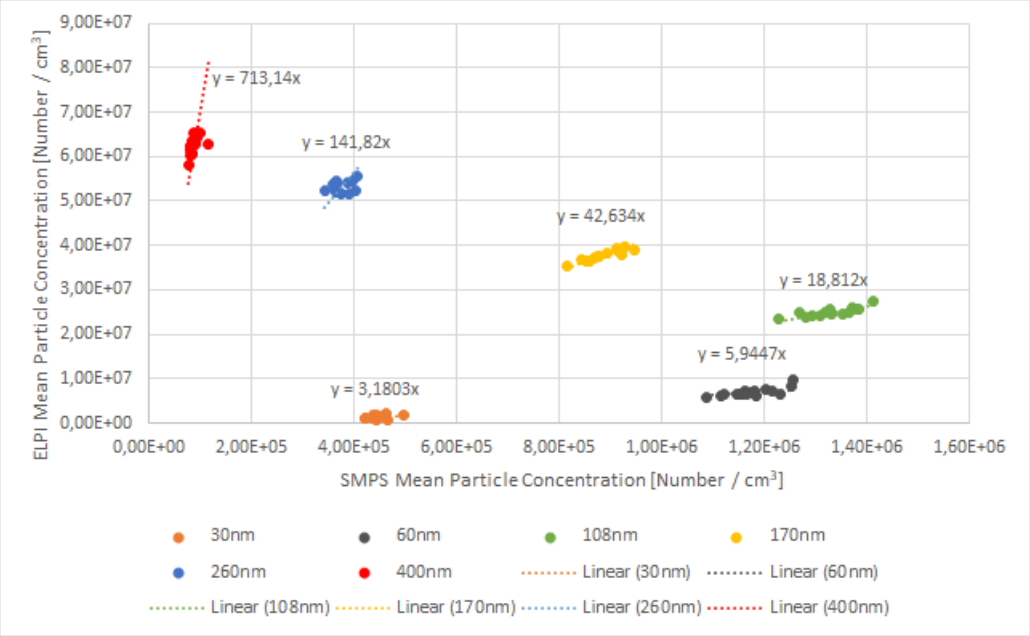

Figure 4.1.2: Correlation factors for SiO_2

Figure 4.1.2 shows scatter plot for silicon dioxide. This chart shows sixteen dots, or time frames for the size groups of 30, 60 and 400 nm and fourteen dots for 108, 170 and 260nm. Each dot represents five consecutive SMPS measurements, twenty five consecutive ELPI+ measurements or 6 minutes and 15 seconds.

This scatter plot 4.1.2 has a higher accuracy as the titanium dioxide chart. A similar observation can be made, that the correlation factor rises with size group, resulting in smaller particles deliver related values and larger particles deliver divergent values.

But the exact values differ greatly, when comparing the same size group from

the titanium dioxide to the silicon dioxide chart. The correlation factor values are depicted as the value of the x variable as part of the linear regression equation.

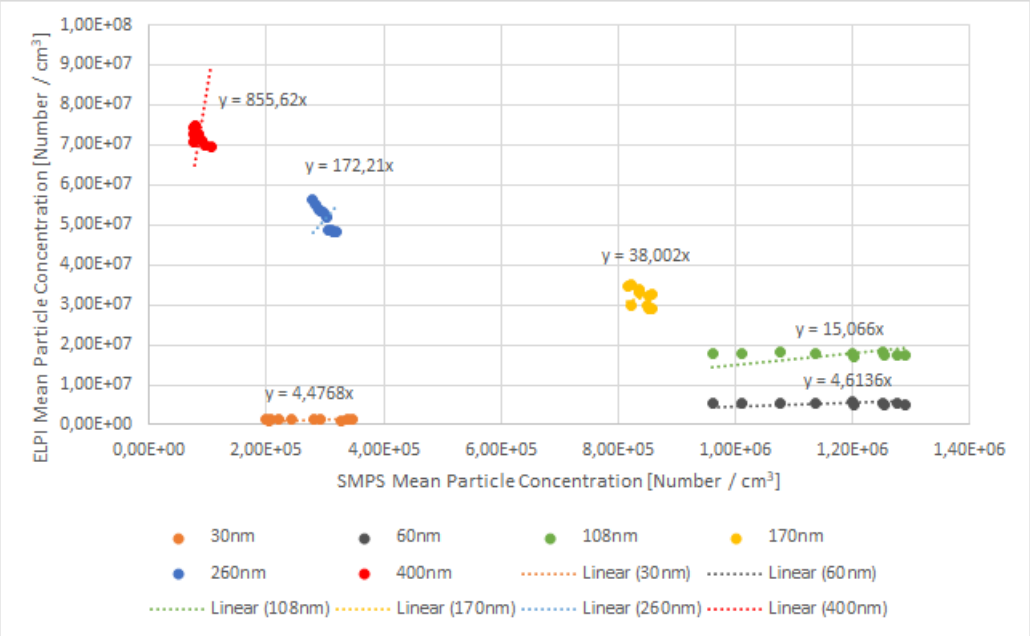

Figure 4.1.3: Correlation factors for ZnO

Figure 4.1.3 shows the scatter plot for zinc oxide. The diagram depicts ten dots or time frames per size group. Each dot represents three consecutive SMPS measurements, fifteen consecutive ELPI+ measurements or 3 minutes and 45 seconds.

Figure 4.1.3 shows that the measuring results have low accuracy, but high similarity at 30, 60 and 108 nm size groups and distinctive higher accuracy, but greatly divergent values at 170, 260 and 400 nm size groups.

The observation made from the charts of TiO_2 and SiO_2 is confirmed in the zinc oxide chart, that both analyser produce coherent data at small particles, but differ greatly the greater the size group gets. Furthermore the correlation factors from zinc oxide are similar to the ones from silicon dioxide.

In conclusion the charts 4.1.1, 4.1.2 and 4.1.3 illustrate, that the ELPI+ and SMPS produce comparable results with varying accuracy and similarity. Furthermore the type of material that is used, which may differ in size distribution, morphology, material parameters, such as density and conductivity, influences

the comparability of these particle analysers. Therefore more experiments can be conducted regarding, mode of operation, analyser geometry, particle concentration and influence from material parameters.

4.2 Collection Efficiency Discussion

The experiment conducted regarding the ability of the *Impinger* to collect and hold different materials is quite interesting. Starting of the discussion with the titanium dioxide measurements.The crude and clean gas depiction 3.3.1 shows the raw particle concentration over the size class, and it is visible that the highest particle concentration is found between 115 and 215 nm. Figure 3.3.2 shows that not all particle sizes are equally well gathered, resulting in a collection efficiency of close to 100% for small particles. Afterwards the collection efficiency decreases to around 70% and stays stable for the rest of the particle sizes.

The silicon dioxide measurement shows a curve trend similar to the titanium dioxide measurement, but the collection efficiency, shown in figure 3.3.4 depicts some irregularities for smaller particles with an efficiency of 86%, which decreases for particles sizes up to 315 nm. From 315 to 615 nm the course is relatively stable at around 50% collection efficiency. Furthermore the crude and clean gas curves have less raw particle counts, compared to the TiO_2 measurement, but the highest value regarding particle size is similar to the TiO_2 value.

The zinc oxide measurement is different to the other measurements. The crude and clean gas curves, depicted in figure 3.3.5, show that the most particles are found between 250 and 300 nm. In addition the overall raw particle value is significantly lower, compared to the other two materials. But the collection efficiency is the best of all three. Close to all small particles are gathered, followed by a slight decrease towards bigger particle sizes, ranging from 130 to 615 nm. The collection efficiency stabilises at around 80%, with an increase towards bigger particles.

All used materials were in general easy to separated from the aerosol flow, with collection efficiency between 50 to 100 %, but with great differences, regarding the size of the particle. On the one hand the smallest particles tend to have the highest collection efficiency, on the other hand the smallest particle sizes are affected by fluctuations of the collection efficiency, resulting in a less stable curve, than bigger

particle sizes. Furthermore the limited solvent present in the wash flask, is quickly saturated with particles. Resulting in a great loss of collection over time. Therefore the measurement was conducted in a duration, when the collection efficiency for the tested materials is at its peak, to show the maximum capacity of the *Impinger*.

5 Summary

This thesis engaged on the task of building an aerosol test device. At first a thorough literature study was conducted and the elaborated results were put into the construction of the aerosol test rig, mainly to fit the requirements of the VDI 3926.

The aerosol test device included an aerosol channel, a pumping system, which sustains the main flow through the device, two aerosol generators, the PALAS AGF 2.0 and the PALAS RBG 2000 and two analysers, the ELPI+ from Dekati and the SMPS from TSI . The device was controlled and monitored by new developed software application written in LabView.

The first experiment conducted on the newly constructed aerosol test device was the production of a stable aerosol flow the PALAS AGF 2.0 and a variety of dust samples, including titanium dioxide, silicon dioxide and zinc oxide. The result show that the duration needed for the each material differ, but that after 25 to 60 minutes, depending on the viewed material, a constant aerosol flow is achieved.

In addition the particle sizes of all three materials were successfully examined and the results were presented. The results showed, that all three dust samples had a unique particle size distributions and that the analysers exhibited some differences, regarding the retrieved values for certain size classes. The differences of both ELPI+ and SMPS were further examined and the discrepancies were fused to a factor, that describes the value difference of different size groups.

The next experiment included the use of a *Impinger* to collect particles in a solvent and test the ability of this wash flask to collect different test dusts, resulting in a collection efficiency for every used material. Therefore the aerosol channel was connected to the wash flask and the aerosol was forced through a layer of vitreous bodies submerged in a liquid medium. The PALAS RBG 2000 generated the necessary aerosol with the dust material titanium dioxide, silicon dioxide and

zinc oxide.

The results showed on the one hand, that the dust samples have their very own collection efficiency curve, which ranges from 50 to nearly 100% collection efficiency and on the other hand, that not all particle sizes are equally good separated from the aerosol flow.

Bibliography

[1] *https://www.meilhaus.de/en/redlab-1208.htm.*

[2] *https://www.palas.de/en/product/rbg2000.*

[3] *National Instruments Homepage: https://www.ni.com/de-at/shop/labview.html.*

[4] Differential Mobility Particle Sizer (Aerosol measurements). Technical report, Eth Zürich, 2014.

[5] Allen, Michael, Raabe, and Otto. Slip correction measurements of spherical solid aerosol particles in an improved Millikan apparatus. *Aerosol Science and Technology*, 4(3):269–286, 1985.

[6] Alton. Characterization of a cesium surface ionization source with a porous tungsten ionizer. I. *Review of scientific instruments*, 59(7):1039–1044, 1988.

[7] Anton Paar, Anton-Parr-Str. 20. *Instruction manual litesizer 500*, March 2016. Anton Paar Litesizer 500 Instruction Manual URL: https://www.utoledo.edu/nsm/ic/pdfs/Litesizer

[8] Ceresana. Titanium Dioxide Market Report (TiO2). 2020.

[9] Donaldson, Bolton, Jones, Brown, Robertson, Slight, Cowie, and Davis. Kinetics of the bronchoalveolar leucocyte response in rats during exposure to equal airborne mass concentrations of quartz, chrysotile asbestos, or titanium dioxide. *Thorax*, 43(7):525–533, 1988.

[10] Emanuelsson. *Formation, ageing and thermal properties of secondary organic aerosol*. University of Gothenburg. Faculty of Science, 2013.

[11] Federici, Shaw, and Handy. Toxicity of titanium dioxide nanoparticles to rainbow trout (Oncorhynchus mykiss): gill injury, oxidative stress, and other physiological effects. *Aquatic toxicology*, 84(4):415–430, 2007.

[12] International Agency for Research on Cancer et al. Iarc monographs on the identification of carcinogenic hazards to humans. In *List Classif. Agents Classif. by IARC Monogr*, volume 1. 2019.

[13] International Organization for Standardization (ISO). Nanotechnologies-Vocabulary-Part 2: Nano-objects. *ISO/TS 80004-2: 2015*, 2015.

[14] Fuchs. On the stationary charge distribution on aerosol particles in a bipolar ionic atmosphere. *Geofisica pura e applicata*, 56(1):185–193, 1963.

[15] Hanley, Thurber, Hanna, Punnoose, Zhang, and Wingett. The influences of cell type and ZnO nanoparticle size on immune cell cytotoxicity and cytokine induction. *Nanoscale research letters*, 4(12):1409, 2009.

[16] Hess-Kosa. *Indoor air quality: sampling methodologies*. CRC Press, 2010.

[17] Höflinger. Skriptum zur Vorlesung Mechanische Verfahrenstechnik I. TU Wien, 2000.

[18] Hunt, McEwen, and Harvey. Positive and negative chemical ionization mass spectrometry using a Townsend discharge ion source. *Analytical Chemistry*, 47(11):1730–1734, 1975.

[19] Malvern Instruments. Mastersizer 2000 user manual. *Worcestershire, United Kingdom: Malvern Instruments*, 2007.

[20] Intra and Tippayawong. An overview of unipolar charger developments for nanoparticle charging. 2011.

[21] A Järvinen, M Aitomaa, A Rostedt, J Keskinen, and J Yli-Ojanperä. Calibration of the new electrical low pressure impactor (elpi+). *Journal of aerosol science*, 69:150–159, 2014.

[22] Dekati Ltd. Elpi Manual. *Tampere, Finland*, 2010.

[23] Maricq, Matti, Podsiadlik, Diane, Chase, and Richard. Size distributions of motor vehicle exhaust PM: a comparison between ELPI and SMPS measurements. *Aerosol Science & Technology*, 33(3):239–260, 2000.

[24] Marple, Liu, and Whitby. Fluid mechanics of the laminar flow aerosol impactor. *Journal of Aerosol Science*, 5(1):1–16, 1974.

[25] Marple and Willeke. Impactor design. *Atmospheric Environment (1967)*, 10(10):891–896, 1976.

[26] Gerd Mauschitz. *Skriptum zur Vorlesung Partikelmesstechnik*. TU Wien, 2010.

[27] McNulty. Production of titanium dioxide. In *Proceedings of NORM V international conference, Seville, Spain*, pages 169–189. Citeseer, 2007.

[28] Scientific Committee on Emerging and Newly Identified Health Risks (SCENIHR). The appropriateness of existing methodologies to assess the potential risks associated with engineered and adventitious products of nanotechnologies, 2006.

[29] Palas GmbH, Greschbachstraße 3 b 76229 Karlsruhe Germany. *Aerosolgenerator*. Palas AGF 2.0 https://www.palas.de/en/product/agf20.

[30] Schladitz. A concept of an automated function control for ambient aerosol measurements using mobility particle size spectrometers. *Atmospheric Measurement Techniques, Volume 7*, 2014.

[31] Heinrich Schubert. On the origin of "anomalous" shapes of the separation curve in hydrocyclone separation of fine particles. *Particulate science and technology*, 22(3):219–234, 2004.

[32] Sievert. *Entwicklung eines unipolaren Aerosolaufladers mit hoher Dynamik zur Bestimmung der Partikelgrößenverteilung am strömenden Aerosol*. Herbert Utz Verlag, 1998.

[33] TSI. Series 3080 Manual. 2009.

[34] Umweltbundesamt. Grenz-, Ziel- und Schwellenwerte. *https://www.umweltbundesamt.at/klima/luftguete-daten/luft-grenzwerte*, 2020.

[35] Unger, Boulaud, and Borra. Unipolar field charging of particles by electrical discharge: effect of particle shape. *Journal of Aerosol Science*, 35(8):965–979, 2004.

[36] Wakamatsu, Morikawa, and Ito. Air pollution trends in Japan between 1970 and 2012 and impact of urban air pollution countermeasures. *Asian Journal of Atmospheric Environment*, 7(4):177–190, 2013.

[37] Wei, Rosario, and Montoya. Collection efficiency of a midget impinger for nanoparticles in the range of 3–100 nm. *Atmospheric Environment*, 44(6):872–876, feb 2010.